



# Natural aporphine alkaloids: A comprehensive review of phytochemistry, pharmacokinetics, anticancer activities, and clinical application



Jing Sun<sup>a,1</sup>, Xingtian Zhan<sup>b,\*,1</sup>, Weimin Wang<sup>a</sup>, Xiaojie Yang<sup>a</sup>, Yichen Liu<sup>a</sup>, Huanzhi Yang<sup>a</sup>, Jianjun Deng<sup>c,d</sup>, Haixia Yang<sup>a,\*</sup>

<sup>a</sup> College of Food Science and Nutritional Engineering, China Agricultural University, Beijing 100083, China

<sup>b</sup> School of Public Administration and Policy, Renmin University of China, Beijing 100872, China

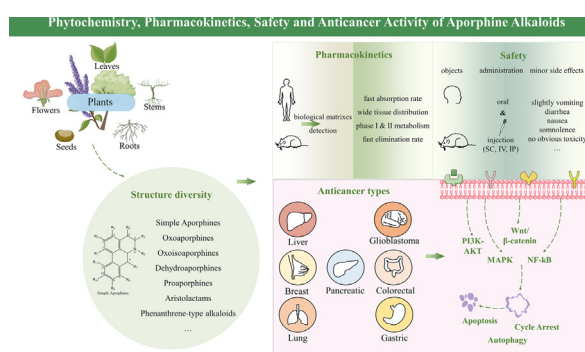
<sup>c</sup> State Key Laboratory of Vegetable Biobreeding, Institute of Vegetables and Flowers, Chinese Academy of Agricultural Sciences, Beijing 100081, China

<sup>d</sup> Shaanxi Key Laboratory of Degradable Biomedical Materials, Shaanxi R&D Center of Biomaterials and Fermentation Engineering, Biotech & Biomed Research Institute, School of Chemical Engineering, Northwest University, Xi'an, China

## HIGHLIGHTS

- The chemical structures and botanical diversity of aporphine alkaloids (AAs) are elucidated.
- Pharmacokinetics and safety of AAs in animals and clinical trials are highlighted.
- Some of AAs exhibit potent anticancer activities.
- Treatment with AAs alone or a synergistic treatment with metal/clinical therapeutic drugs shows initial therapeutic promise.
- AAs is the potential ingredient to develop the functional food containing plant-derived AA and the clinical application of AAs.

## GRAPHICAL ABSTRACT



## ARTICLE INFO

### Article history:

Received 30 July 2023

Revised 17 October 2023

## ABSTRACT

**Background:** Cancer is the most common cause of death and is still a serious public health problem. Alkaloids, a class of bioactive compounds widely diffused in plants, especially Chinese herbs, are used as functional ingredients, precursors, and lead compounds in food and clinical applications. Among them,

**Abbreviations:** AAs, Aporphine alkaloids; AKT, protein kinase B; AMPK, AMP-activated protein kinase; Apaf-1, the apoptotic protease activating factor-1; AhR, the aryl hydrocarbon receptor; BCRP, breast cancer resistant protein; BMICs, brain metastasis initiating cells; BBB, blood–brain barrier;  $C_{max}$ , maximum plasma concentration; CYP, cytochrome P450; UGT, uridine diphosphate glycosyltransferase; CDK1/2, cyclin dependent kinases 1/2; COMT, catechol-O-methyl transferase; EMT, epithelial-to-mesenchymal transition; ERK, extracellular signal-regulated kinases; EGFR, epidermal growth factor receptor; F, oral absolute bioavailability; GSK-3 $\beta$ , glycogen synthase kinase 3 $\beta$ ; HSCCC, high-speed counter-current chromatography; HMGCR, 3-hydroxy-3-methyl-glutaryl-coA reductase; HIF-1 $\alpha$ , hypoxia-inducible factor-1  $\alpha$ ; hTERT, human telomerase reverse transcriptase; ILMAE, ionic liquids-based microwave-assisted extraction; IV, intravenous injection; IP, intraperitoneal injection; IL, interleukin; SC, subcutaneous injection; JNK, stress-activated protein kinases; mTOR, mechanistic target of rapamycin; MAPKs, Mitogen-activated protein kinases; MET, mesenchymal-to-epithelial transition; NF- $\kappa$ B, nuclear factor  $\kappa$ B; NADES, the natural deep eutectic solvents; Nrf2, the nuclear factor E2-related factor 2; PDCD4, the programmed cell death 4; PARP, the poly ADP ribose polymerase; 53BP1, p53-binding protein 1; PI3K, phosphatidylinositol 3-kinase; P-gp, P-glycoprotein; PXR, the pregnane X receptor; ROS, reactive oxygen species; STAT3, activator of transcription 3; SOX2, sex determining region Y (SRY)-box 2;  $T_{max}$ , time to reach concentration peak; TNF- $\alpha$ , tumor necrosis factor  $\alpha$ ; TLR4, Toll-like receptor 4; TMEM16A, the transmembrane protein 16A; UAE-SPE, ultrasonic-assisted extraction-solid phase extraction;  $V_d$ , apparent volume of distribution; VEGF-A, vascular endothelial growth factor A; YAP, YES-associated protein Ser127.

\* Corresponding authors.

E-mail addresses: [ruczhanxt@163.com](mailto:ruczhanxt@163.com) (X. Zhan), [hyang@cau.edu.cn](mailto:hyang@cau.edu.cn) (H. Yang).

<sup>1</sup> These authors contributed equally to the work.

<https://doi.org/10.1016/j.jare.2023.11.003>

2090-1232/© 2024 The Authors. Published by Elsevier B.V. on behalf of Cairo University.

This is an open access article under the CC BY-NC-ND license (<http://creativecommons.org/licenses/by-nc-nd/4.0/>).

Accepted 3 November 2023  
Available online 5 November 2023

#### Keywords:

Aporphine alkaloids  
Anticancer  
Phytochemistry  
Pharmacokinetics  
Application

aporphine alkaloids (AAs), as an important class of isoquinoline alkaloids, exert a strong anticancer effect on multiple cancer types.

**Aim of review:** This review aims to comprehensively summarize the phytochemistry, pharmacokinetics, and bioavailability of seven subtypes of AAs and their derivatives from various plants and highlight their anticancer bioactivities and mechanisms of action.

#### Key Scientific Concepts of Review.

The chemical structures and botanical diversity of AAs are elucidated, and promising results are highlighted regarding the potent anticancer activities of AAs and their derivatives, contributing to their pharmacological benefits. This work provides a better understanding of AAs and combinational anticancer therapies involving them, thereby improving the development of functional food containing plant-derived AA and the clinical application of AAs.

© 2024 The Authors. Published by Elsevier B.V. on behalf of Cairo University. This is an open access article under the CC BY-NC-ND license (<http://creativecommons.org/licenses/by-nc-nd/4.0/>).

## Contents

Introduction . . . . .	232
The phytochemistry of AAs . . . . .	233
Structural diversity of AAs . . . . .	233
Botanical sources of AAs . . . . .	237
Extraction, purification, and identification of AAs . . . . .	237
Pharmacokinetics of AAs . . . . .	238
Absorption . . . . .	240
Distribution . . . . .	241
Metabolism . . . . .	242
Safety . . . . .	243
Anticancer activities of AAs on cancer . . . . .	243
Anti-cancer effect of AA alone . . . . .	243
Structure-anticancer activity relationship: Role of the C8 position of AAs . . . . .	245
Synergistic anticancer bioactivities . . . . .	245
Strategies of AA-delivery system for application . . . . .	246
Mechanism of action of AAs against cancer . . . . .	246
PI3K-AKT signaling pathway . . . . .	246
MAPK signaling pathway . . . . .	247
Wnt/ $\beta$ -catenin signaling . . . . .	248
NF- $\kappa$ B signaling pathway . . . . .	248
Cell autophagy, apoptosis, and cycle arrest . . . . .	248
Regulation of gut microbiota . . . . .	249
Other signaling pathways . . . . .	249
Conclusion . . . . .	249
CRedit authorship contribution statement . . . . .	249
Declaration of Competing Interest . . . . .	249
Acknowledgement . . . . .	249
References . . . . .	249

## Introduction

Cancer has become globally public health and economic problems caused by its serious morbidity and mortality. In 2022, approximately 4.8 million and 2.3 million new cancer cases, and 3.2 million and 0.6 million cancer deaths occurred in China and the USA, respectively [1]. Apart from the genetic risks, epidemiological studies showed that lifestyle, including smoking, excessive alcohol consumption, unhealthy dietary pattern, and physical inactivity, is associated with high cancer risk [2,3]. As the field has evolved in cancer research and understanding in recent years, therapeutic options for cancer treatment include surgery, chemotherapy, and radiotherapy, which are accompanied by many side effects, such as incomplete removal of the tumor, metastasis development, recurrence, chronic pain and drug resistance. Researchers are now focusing on the use of natural phytochemicals, which show beneficial effects on cancer prevention and treatment with low toxicity [4–6].

Natural compounds are considered as promising strategies for cancer and inflammatory diseases [7–9]. The discovery of phytotherapy dates back to ancient Mesopotamia about 2,600 BCE. From 1980s, natural product drugs of the global approved antitumor drugs accounts for 33.5 % [7,10]. Notably, alkaloids have attracted tremendous attention due to their wide clinical application. For example, Taxol/paclitaxel, as a diterpene alkaloids derived from the bark of the yew tree *Taxus brevifolia* Nutt., was approved as chemotherapy drug in 1993 for treatment of various cancers including breast, ovarian, pancreatic and prostate cancer [10–12]. Besides, natural alkaloids such as vinblastine and vincristine, and their derivatives vindesine and vinorelbine are anticancer drugs in clinic, showing bioactivities against neoplasms, chorio carcinoma hodgkins disease and non small cell bronchial carcinoma [10,13].

Aporphine alkaloids (AAs, also called aporphinoids) are a class of isoquinoline alkaloids generally characterized by a tetracyclic aromatic basic N-containing skeleton (shown in Fig. 1) [14]. AAs

are secondary metabolites found common throughout the plant kingdom, including Nymphaeaceae, Ranunculaceae and Annonaceae [15–17]. The applications of AAs in clinic dates back to the Qin and Han Dynasties, known as preventing fevers and insomnia with dietary herbal medicines such as lotus leaf, as recorded in “*Shenmng Bencao Jing*” [18]. Actually, different active AAs has been identified and explored (shown in Table 1). AAs significantly inhibited the initiation, development and metastasis of tumor by regulating cellular functions and immune response, such as perturbation of cell cycle, programmed cell death and pro-inflammatory cytokines [2,19–21]. AAs also play the key role in inhibiting the cancer cell proliferation through glycolytic pathway [22].

The relationship between the structure and bioactivities, especially anticancer effects, as well as the potential mechanisms of AAs are not well summarized because of the diversity of their chemical structures. This review summarizes the basic information of AAs, including their structures, botanical origins, and pharmacokinetics, as well as their anticancer activities and the mechanisms of action, to provide a theoretical basis in the application of AAs in clinical practice and food industry.

All available information on AAs was collected from scientific databases, including PubMed, Web of Science, ScienceDirect, Scopus, Springer, ACS, Wiley, and Google Scholar. The search terms used for this review included aporphine alkaloids, phytochemistry, pharmacokinetics, toxicity, anticancer, antitumor, and mechanism. The screening process of all papers primarily relied on reviewing their titles and abstracts and only articles in English were considered for inclusion in this review. Inclusion criteria were phytochemical property, clinical, *in vivo*, and *in vitro* researches on pharmacokinetics, toxicity, anticancer activities and mechanism.

Exclusion criteria encompassed studies that focused on synthetic products or did not directly address the topic.

## The phytochemistry of AAs

### Structural diversity of AAs

AAs are mainly classified into seven subtypes based on various substitution and planar conformations, such as simple aporphines, oxoaporphines, oxoisoaporphines, dehydroaporphines, proaporphines, aristolactams, and phenanthrene-type alkaloids (Fig. 1). Simple aporphines are the most common subclasses of AAs, with a 5,6,6a,7-tetrahydro-4H-dibenzo[de.g]quinoline core, accompanied by various substitution groups at various positions (including hydroxyl, methoxy, methylenedioxy, and carbonyl group) [16]. Nitrogen is actively substituted with groups, including methyl or aldehyde, or cyanide (Fig. 1A). Among them, the N-methyl and N-(2-hydroxypropyl) substitution groups on the basic skeleton of simple aporphines, such as nuciferine and (+)-N-(2-hydroxypropyl) lindcarpine, are beneficial groups in terms of cytotoxicity on cancer cells [23]. Apomorphine, a semi-synthetic drug currently used to treat Parkinson's disease, has one tertiary amine (aliphatic) and two aromatic hydroxyls, which is produced by reacting morphine with  $ZnCl_2$  or hydrochloric acid. Moreover, the structural modifications of simple aporphines have attracted researchers' attention and new lead molecules containing a C10 nitrogen motif are synthesized and acting as the neurotransmitter serotonin receptors to resolve neuropsychiatric conditions [24].

Oxoaporphines and oxoisoaporphines are the derivatives of 1-azabenzanthrone that is composed of an aromatic quinoline ring

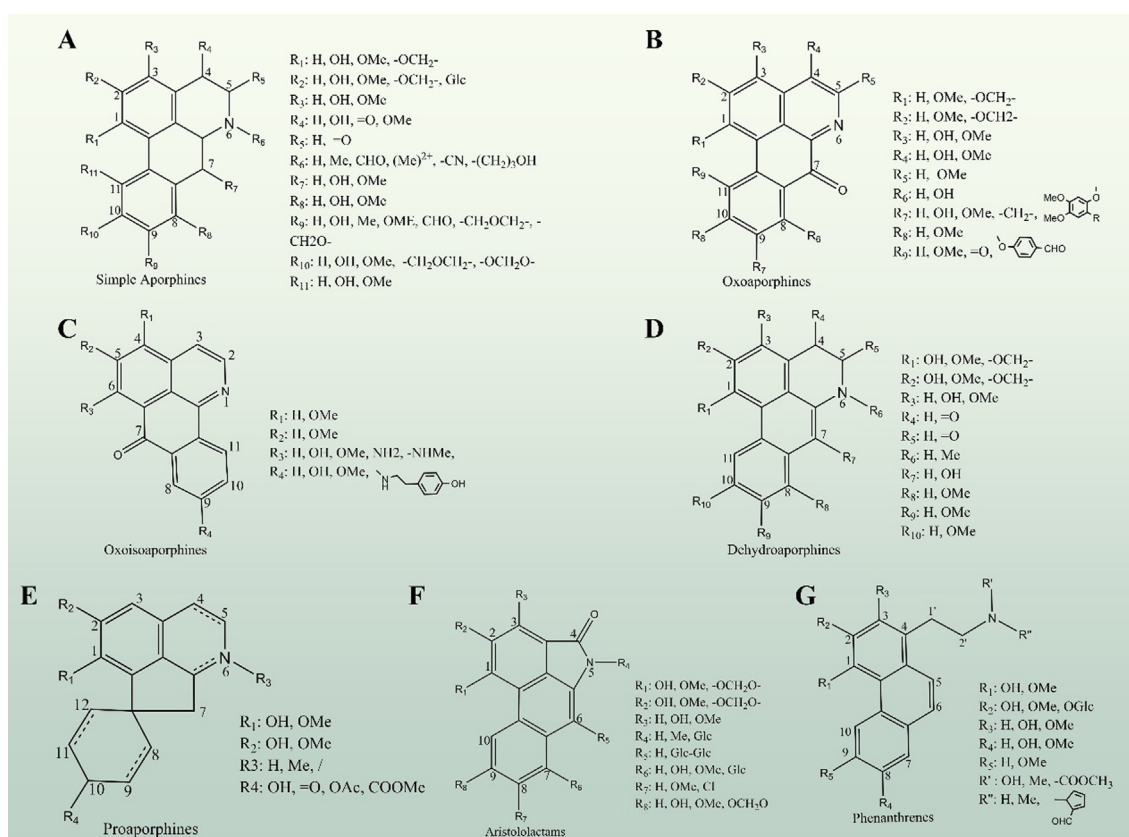


**Fig. 1.** The basic skeleton of AAs, involving simple aporphines (A), oxoaporphines (B), oxoisoaporphines (C), dehydroaporphines (D), proaporphines (E), aristolactams (F), and phenanthrene (G) alkaloids.

**Table 1**  
Natural sources of AAs with anticancer activity.

Botanical family	Plant name	Aporphine type	Compound name	Parts	Content (mg/kg)	Ref.		
Nymphaeaceae	<i>Nelumbo nucifera Gaertn</i> (called lotus)	Simple aporphines	anonaine	leaves	3.3	[41]		
			asimilobine		2.7			
			caaverine		2.7			
			N-methylasimilobine		10.7			
			nuciferine		13.3			
			nornuciferine		11.3			
		roemerine	4.0					
		oxoaporphines	liriodenine		2.7			
			lysicamine		10.0			
		dehydroaporphines	7-hydroxydehydronuciferine		8.0			
			cepharadione B		10.0			
		simple aporphines	nuciferine		flower buds		42.2	[34]
			nornuciferine				7.7	
	N-methylasimilobine		17.5					
	proaporphines	asimilobine	leaves and flower buds	9.7	[42]			
		pronuciferine		15.2				
	simple aporphines	nuciferine	leaves and flower buds	74.8 ~ 92.2; 148 ~ 203.3	[42]			
		N-nornuciferine		2.6; 11.2 ~ 134.4				
		N-methylasimilobine		313.3; 6.6 ~ 40				
		N-methylasimilobine N-oxide		3.7; -				
		nuciferine N-oxide		24.6 ~ 45.2; -				
		asimilobine		165.6; -				
		(-)-lirinidine		8.0; 3.3				
oxoaporphines		lysicamine		3.3 ~ 46.4; 36.5 ~ 102				
proaporphines		pronuciferine		9.2; 25.6 ~ 56				
dehydroaporphine		dehydronuciferine		4.3; -				
Ranunculaceae	<i>Thalictrum wangii</i>	simple aporphines	2-hydroxy-1-methoxy-6a,7-dehydroaporphine	whole plants	3.2; -	[134]		
			(+)-8-(4'-formylphenoxy)glaucine		2.5			
			(+)-8-(4'-hydroxymethylphenoxy)glaucine		7.9			
			(+)-3-methoxy-8-(4'-formylphenoxy)glaucine		2.2			
		oxoaporphines	1,2,3,9,10-pentamethoxy-11-(4'-formylphenoxy)-7-oxoaporphine		0.9			
			1,2,9,10-tetramethoxy-11-(4'-formylphenoxy)-7-oxoaporphine		0.5			
		proaporphine	10-O-acetyl prodensiflorin A		1.7 ~ 2.3			
			simple aporphines		(-)-9-(2'-methoxycarbonyl-5', 6'-dimethoxyphenoxy)-1, 2, 3, 10-tetramethoxy aporphine		roots	6.0
	(-)-2'-methoxycarbonyl thaliadin	2.8						
	(-)-9-(2'-methoxyethyl-5', 6'-dimethoxyphenoxy)-1, 2, 3, 10-tetramethoxy aporphine	0.3						
	(-)-3-methoxy hydroxyhernandalinol	0.2						
	thaliadine	1.1						
	oxoaporphines	9-(2'-formyl-5', 6'-dimethoxyphenoxy)-1, 2, 3, 10-tetramethoxy oxoaporphine		0.4				
	dehydroaporphine	3-methoxy-2'-formyl oxohernandalin		1.9				
		9-(2'-formyl-5', 6'-dimethoxyphenoxy)-1, 2, 3, 10-tetramethoxy dehydroaporphine		0.1				
	<i>Thalictrum cultratum</i>	dimeric aporphine alkaloids	3-methoxydehydrohernandaline	roots	0.2	[36]		
thalicultrate			0.4 ~ 17.5					
thalifaronine			2.7					
thalifaberine			5.2					
thalifabatine			5.6					
dehydrothalifaberine			2.1					
thalibealine			0.8					

Table 1 (continued)

Botanical family	Plant name	Aporphine type	Compound name	Parts	Content (mg/kg)	Ref.	
Annonaceae	<i>Fissistigma glaucescens</i> (Hance) Merr	simple aporphines	(+)-nornuciferine	stems	1.4	[43]	
			norisocorydine		1.5		
			laurotetanin		1.8		
		<i>Enicosanthellum pulchrum</i> (King) Heusden	oxoaporphines	Aporaloid	roots	1.2 ~ 1.3	[25]
			oxoxylopin	15.3			
			micheline B	2.3			
		<i>Pseuduvaria trimera</i> (Craib)	dehydroaporphines	norcepharadione	leaves and twigs	8.6	[135]
			oxoaporphines	liriodenine		80	
		<i>Xylopia laevigata</i>	oxoaporphines	8-hydroxyartabonatin C (6a,7-dehydro-1,4,5-trimethoxy-7-oxoaporphine)	stems	52.0	[101]
			dehydroaporphines	ouregidione		12.6	
	simple aporphines		(-)-Roemerine	2.7			
			(+)-Anonaine	5.0			
			(+)-Glaucine	0.7			
			(+)-Xylopine	9.6			
			(+)-Norglaucine	5.9			
			Asimilobine	0.5			
			(+)-Norpurpureine	3.1			
			(+)-N-methylaurotetanine	3.9			
		(+)-Norpredicentrine	5.1				
		(+)-Calycinine	1.1				
		(+)-Laurotetanine	5.9				
		oxoaporphines	Lanuginosine	3.6			
			Oxoglaucine	5.9			
Lauraceae	<i>Goniothalamus laoticus</i>	simple aporphines	(-)-nordicentrine	flowers	17.9	[136]	
		simple aporphines	(+)-6S-ocoteine N-oxide	leaves and trunk barks	50.0	[137]	
	<i>Ocotea acutifolia</i> (Nees) Mez.		norocoxylonine	13.0			
			(+)-6S-dicentrine N-oxide	10.0			
			(+)-ocoteine	42.0			
			(+)-ocoxylonine	14.0			
			O-methylcassyfiline	14.0			
			(+)-dicentrine	20.0			
			leucosine	14.0			
			(+)-thalicsimidine	8.0			
	(+)-isodomes ticine	12.8					
		neolitsine	10.6				
		halicminine	30.0				
papaveraceae	<i>Dehaasia longipedicellata</i>	oxoaporphines	boldine	barks	5.0	[138]	
	<i>Dicranostigma leptopodum</i> (Maxim) Fedde	simple aporphines	norbaldine		5.0		
		simple aporphines	Isocorydione	whole plants	1250	[35]	

(continued on next page)

Table 1 (continued)

Botanical family	Plant name	Aporphine type	Compound name	Parts	Content (mg/kg)	Ref.	
Menispermaceae	<i>Stephania dielsiana</i> Y.C. Wu	oxoaporphines	oxostephanine	leaves	1.2	[127]	
		simple aporphines	crebanine	leaves	40.2	[139]	
	<i>Stephania venosa</i> (Blume) Spreng	oxoaporphines	oxostephanine			5.2	
		dehydroaporphine	thailandine			26.2	
	<i>Stephania venosa</i> (Blume) Spreng	dehydroaporphine	4,5-dioxo-dehydrocrebanine			11.0	
			dehydrocrebanine (2)			8.9	[140]
		simple aporphines	stephanine 3			37.5	
			crebanine 4			58.3	
			O-methylbulbocapnine 5			91.7	
	<i>Sinomemium acutum</i>	dehydroaporphine	dehydrocrebanine 1			55.8	
		simple aporphines	magnoflorine			388.8	[40]
		oxoisoaporphines	dauriporphine	stems and rhizomes		25.6	
			bianfugicine			0.8	
	<i>Formosan Coccullus orbiculatus</i> <i>Magnolia grandiflora</i> L.	simple aporphines	dauriporphinoline			5.6	
			menisporphine			4.0	
		simple aporphines	(+)-laurelliptimhexadecan-1-one			0.2	[40]
			(+)-laurelliptimoctadecan-1-one			0.2	
			magnoflorine			3.3	[39]
	oxoaporphines	anonaine			2.2		
lanuginosine				3.9			
			liriodenine		2.2		

attached to a tetralone unit. Unlike simple aporphines, oxoaporphines, and oxoisoaporphines have an aromatic N-containing ring and a carbonyl group at C7 position in the tetracyclic skeleton (Fig. 1B and C) [16]. According to studies on oxoaporphines activity, both liriodenine and dicentrinone have strong anti-protozoal and anti-cancer activities, suggesting that the oxo-group and 1, 2-methylenedioxy group are the key factors in the action of alkaloids [25]. Although the oxo-group highly improves the conjugation stability of oxo-AAs, a series of new derivatives, which contain a substitution of various amide groups at C4 and C5 position, are synthesized to enhance their cytotoxicity and inhibit bioactivity of topoisomerase [26]. Besides carbonyl substitution at the C7 position, hydroxyl or methoxy groups are sometimes present, known as 7-oxygenated aporphines.

Different from the precedent subtypes, dehydroaporphines have a 5,6-dihydro-4H-dibenzo [de, g] quinoline core with a double bond between C6a and C7 obtained through dehydrogenation, which provides sufficient nucleophilicity to dehydroaporphines for the introduction of carbon substituents (Fig. 1D) [16]. Interestingly, the study of the compounds didehydroglaucine and dehydrocrebanine revealed that the double bond at C6a and C7 plays a critical role in increasing cytotoxicity besides of the 1,2-methylenedioxy group [16]. Moreover, the substitution of the methyl (C1, C2), methoxy (C9, C10), and aldehyde group (nitrogen) at various positions of the dehydroaporphines forms an amidic dehydroaporphine, which possesses wide pharmacological activity *in vivo* and *in vitro*.

Proaporphines are the biogenetic precursors to some specific AAs and are characterized by a new skeleton of an isoquinoline part fused to a pentacyclic ring and then sequentially connected to a benzyl part through a spiro carbon. Proaporphines generally show a substitution by hydroxyl, methoxy and methyl group at C1, C2, C10 position, and the methyl at N-atom occasionally forms double bonds through dehydrogenation, as shown in Fig. 1E by a dotted line. The naturally occurring proAA stepharine, which possesses antihypertensive activity and sedative effect, has 1,2-methoxy and carbonyl groups at C10 position, double bonds at C8 and C9, as well as C10 and C12 [27]. Nowadays, more natural proaporphines are consecutively extracted and identified from the plant kingdom, such as cissamaline, cissamanine, and cissamdine, isolated from the leaves and stems of *Cissampelos capensis*, consisting of three ring systems with various substitution groups at C1, C1a, C2, and nitrogen [28].

The basic skeleton of aristolactams (also called aristolactams) shows similarity to that of simple aporphines but with a unique structure in the N-containing ring (Fig. 1F). As a variety of aristolochic acid analogues, aristolactams have a phenanthrene chromophore and exert more potent bioactivities than aporphines due to the presence of the lactam group (typical -CONH- structure) at the N-containing ring [29]. It is well known that aristolactam alkaloids are not confined to the Aristolochiaceae, such as compounds identified in *Fissistigma* species (Annonaceae), including aristolactam AII, BII, and FII, which are substituted by a methoxy group at C1 and/or C2 position, and by a hydroxyl group at C2 and/or C9 position. Aristolactam alkaloids are further classified into four categories according to the difference in oxygenation pattern: dio- (such as 10-Amino-2,4-dimethoxy-phenanthrene-1-carboxylic acid lactam 1), trio- (such as 10-Amino-1-carboxy-3,4-dimethoxy-6-hydroxyphenanthrene lactam N-β-D-glucopyranoside), tetrao- (such as aristolamide-N-hexoside), and pentao-xxygenated (such as 7-Methoxyaristolactam IV) aristolactams. Most of these compounds possess antitumor activities against human cancer cells [29].

Fig. 1G shows the basic skeleton of phenanthrene-type alkaloids, which have an N-containing side chain with various substitutions. The phenanthrene-type alkaloids are generally replaced by hydroxyl and methoxy groups in the aromatic rings (known as

electrophilic substitution reaction). The phenanthrene alkaloid atherosperminine is characterized by a methoxy substitution in C1 and C2 position, and two methyl groups in the N-atom, conferring the ability to strongly inhibit arachidonic acid-induced platelet aggregation [30]. The phenanthrene-type alkaloids originated from the same plants may have a similar structure, such as the compound atherosperminine, 2-hydroxyathersperminine, and noratherosperminine, which are isolated from the bark of *Cryptocarya nigra* and consistently presenting a substitution by methoxy groups at C1 and C2, although they are distinguished by the presence of a hydroxyl group at C3, and methyl groups at the N-atom [31].

However, the basic skeletons of AAs are not limited to those in Fig. 1A–G, for example, compound taspine that has a dilactonic, tertiary amine structure and dimethylaminoethyl side-chain. Besides carbonyl substitution at the C7 position, hydroxyl or methoxy groups are present, known as 7-oxygenated aporphines [32]. Besides, Ali et al. obtained a set of dimeric AAs, which consist of two aporphinoid units through either an ether or less frequently a C–C bond, such as dehatriline with isocorydine and N-methyl-laurotetanine units with an ether linkage [33]. Therefore, AAs exhibit structural diversity, which is helpful in developing clinical drugs to combat various cancers based on the original natural compounds (Fig. 2).

#### Botanical sources of AAs

AAs are primarily distributed within the families of Annonaceae, followed by Ranunculaceae, Nymphaeaceae, Lauraceae, papaveraceae, Menispermaceae and Magnoliaceae, which include various Chinese medicinal plants such as *Nelumbo nucifera Gaertn* [34], *Thalictrum foetidum* [35], and *Thalictrum cultratum* [36,37]. Notably, AAs, such as nuciferine, pronuciferine, and dehydronuciferine, are potential characteristic ingredients in Nymphaeaceae (especially in lotus), while isocorydine is exclusively detected in Papaveraceae compared to other families. This indicates variations in compound distribution among different botanical families

(Table 1). Furthermore, the content of compounds isolated from various plants or plant parts differs significantly. For instance, liriodenine, as an oxoAA, is more abundant in the roots of *Enicosanthellum pulchrum (King) Heusden* (80 mg/kg) than in other plants (<11 mg/kg) [25,38,39], and magnoflorine as a simple AA is richer in the stems and rhizomes of *Sinomenium acutum* (388.8 mg/kg) than in the leaves of *Magnolia grandiflora L.* (3.3 mg/kg) [39,40]. Table 1 shows that the simple AA nuciferine is present in higher content in the flower buds (42.2 mg/kg) than that in the leaves (11.3 mg/kg) of *N. nucifera Gaertn* (called lotus), and the results are consistent with those of Nakamura et al. (148 ~ 203.3 mg/kg in flower buds and 74.8 ~ 92.2 mg/kg in leaves) [34,41,42]. To date, the structural compositions of new AAs from different plant parts have been widely reported, providing sufficient information for the identification and the discovery of new drugs, highlighting the biological diversity and pharmacological value of these natural products.

#### Extraction, purification, and identification of AAs

Considering the promising pharmacological effects of AAs from different plants, efficient extraction, purification, and identification of AAs are critical for research and application. Many strategies have been established not only classical approaches, but also green extraction techniques (Fig. 2).

The classical approach for AA extraction from the plants usually use organic solvents. Plant grounds into powder and macerated with organic solvents including methanol, ethanol, n-hexane or ethyl acetate. Macroporous adsorption resin is employed to enrich the crude extracts followed by dissolving in acidic solution, normally hydrochloric acid or acetic acid, to solubilize the alkaloids [43]. The extraction efficiency of AAs with organic solvent is impacted by parameters, such as solvent, temperature, pressure, and extraction time. Considering that AAs are a group of compounds sensitive to both light and heat, these factors present notable challenges during the extraction procedure [37]. Following extraction using acidic and basic solutions, the crude AAs extracts

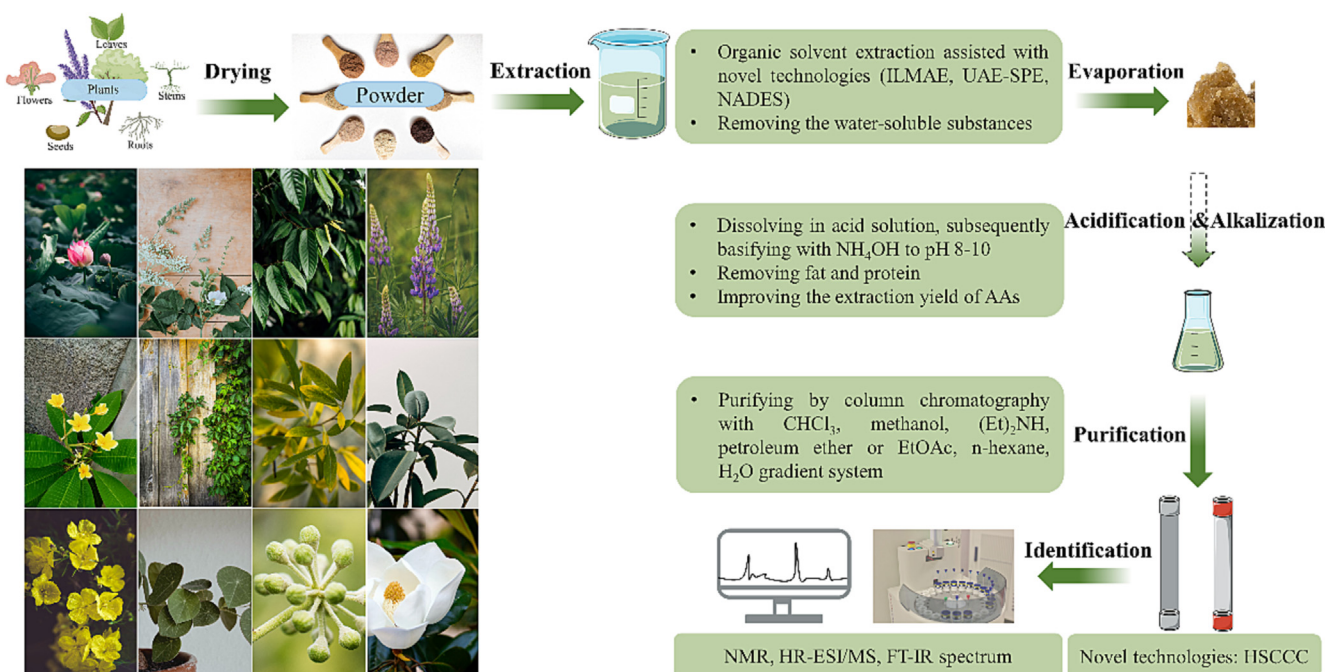


Fig. 2. The plant species and schematic representation of the extraction, purification, and identification of AAs. ILMAE: ionic liquids-based microwave-assisted extraction; UAE-SPE: ultrasonic-assisted extraction-solid phase extraction; HSCCC: high-speed counter-current chromatography; NADES: natural deep eutectic solvents.

are subjected to silica gel column chromatography with gradient elution, commonly involving  $\text{CH}_2\text{Cl}_2$ -MeOH,  $\text{CHCl}_3$ -MeOH,  $\text{CH}_3\text{-COOCH}_3$ -MeOH, MeOH- $\text{H}_2\text{O}$  and petroleum ether- $\text{CH}_3\text{COOCH}_3$  gradient system [25]. The choice of eluents in chromatography is determined by the polarity of AAs. Identification is performed by using semi-preparative high-performance liquid chromatography (HPLC) in combination with spectroscopic assays, such as hydrogen nuclear magnetic resonance ( $^1\text{H NMR}$ ), carbon-13 nuclear magnetic resonance ( $^{13}\text{C NMR}$ ), high-resolution electrospray ionization mass spectrometry (HR-ESI/MS), and fourier-transform infrared spectroscopy (FT-IR).

Moreover, the potential of green extraction techniques as an alternative to traditional extraction approaches has been extensively explored. One green extraction strategy is the use of non-toxic solvents, such as natural deep eutectic solvents (NDES) and supercritical carbon dioxide ( $\text{Sc-CO}_2$ ). NDES have gained increasing attention benefited from their simple preparation, low cost, biodegradability, sustainability, high solubilization power and acceptable pharmaceutical toxicity [44–46]. Menthol-camphor and menthol-thymol NDES mixtures yielded high amounts of chelidonine (35 %), berberine (76 %), and coptisine (180 %) compared with control extractants (water and methanol) in the extraction of *Chelidonium majus* plant [45]. Besides, the boldine extraction with proline-oxalic acid NDES mixture is eight-times more efficient than methanol in *Peumus boldus* Mol., (Monimiaceae) [46]. Choline chloride-fructose NDES mixture demonstrated a total alkaloidal extraction capacity of 2.43, 2.25 and 2.38 times than that of ethanol, methanol and water, respectively [47].  $\text{Sc-CO}_2$  is commonly used in supercritical fluid extraction (SFE) due to its gas-like and liquid-like properties, selectivity in extracting specific compounds and can be easily removed by depressurization [48,49]. In recent years,  $\text{Sc-CO}_2$  extraction is used to obtain the

alkaloids from plants, such as *Sophora moorcroftiana*, *N. tabacum* leaves and *Camellia sinensis* (L.) Kuntze [50–52].

Other green extraction strategies are extraction combined with innovative technologies including ionic liquids-based microwave-assisted extraction (ILMAE), ultrasonic-assisted extraction-solid phase extraction (UAE-SPE), and pressurized liquid extraction (PLE) [52–55]. Ionic liquids have been successfully applied in two-phase systems extraction due to their unique properties of negligible vapor pressure and volatility, high thermal stability and ease of handling. In the alkaloids extraction from lotus leaves, the application of ILMAE, specially 1-hexyl-3-methylimidazolium bromide as the ionic liquids, resulted in 26 % enhancement in efficiency and reduction in extraction time (from 2 h to 2 min) compared to the regular MAE technique [56]. UAE has been frequently assisted with various extraction solvents while UAE-SPE is successfully applied in production of high purity nuciferine with a purity over 98.5 % from lotus leaves [57]. Pretreatment such as concentration or re-dissolving before SPE is not required, and waste solvents from SPE can be used as UAE extractants without purification, resulting in significant energy and emission reductions [57]. Under high temperature and pressure conditions, the use of PLE effectively improves the compounds solvation and diffusion rates, simultaneously shorts the extraction time and reduce the solvent consumption [58]. PLE is generally targeted at polar compounds extraction and has been successfully used to extract alkaloids, such as caffeine and theobromine from cocoa shell [59].

### Pharmacokinetics of AAs

The pharmacokinetics of AAs has attracted considerable scientific attention due to the multiple bioactivities of AAs identified

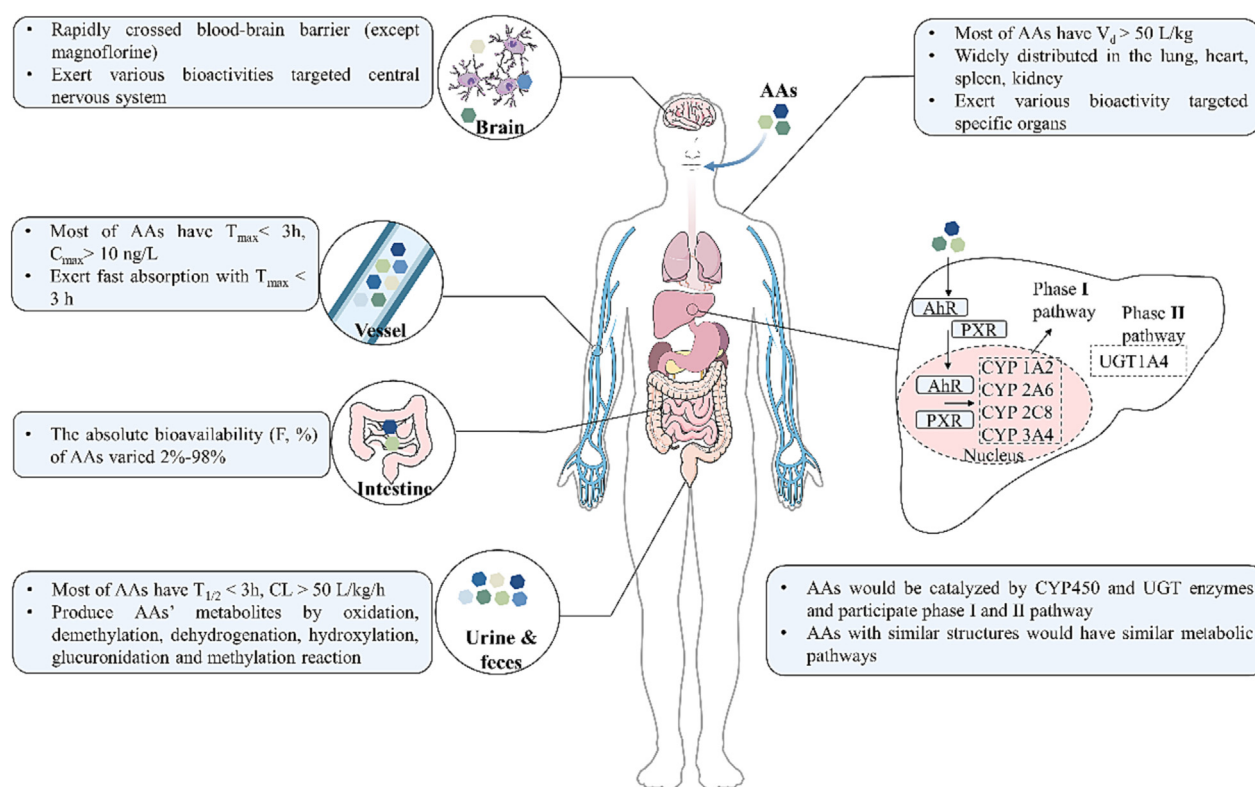


**Fig. 3.** The absorption, distribution, metabolism, and excretion properties of AAs. AAs: aporphine alkaloids; AhR: the aryl hydrocarbon receptor;  $C_{\max}$ : maximum plasma concentration; CL: clearance rate; CYP: cytochrome P450; F: oral absolute bioavailability; PXR: the pregnane X receptor;  $T_{\max}$ : time to reach concentration peak;  $T_{1/2}$ : terminal elimination half-life; UGT: uridine diphosphate glycosyltransferase;  $V_d$ : apparent volume of distribution.



**Table 2**  
Pharmacokinetic parameters of AA in various models.

Name	Model	Dose	Treatment	C <sub>max</sub> /ng/mL	T <sub>max</sub> (h)	T <sub>1/2</sub> (h)	AUC <sub>0</sub> <sup>t</sup> h*ng/mL	AUC <sub>0</sub> <sup>∞</sup> h*ng/mL	CLL/kg/h	V <sub>d</sub> L/kg	F/%	Ref
apomorphine	PD Patients (no smoking, 30–85 years old, BMI = 18–32 kg/m <sup>2</sup> )	2–4 mg/kg	oral once daily for 1–5 days	6.9–9.6 (2 mg/kg); 12–19.3 (3 mg/kg); 14.9–28.1 (4 mg/kg)	1–2	0.6–0.7	–	2.3–2.6 (2 mg/kg); 4.5–7.1 (3 mg/kg); 5.7–8 (4 mg/kg)	–	–	–	[141]
		20–30 mg/kg	sublingual film	4.3–11.2	0.6–0.8	1.1–1.2	7.2–22.8	7.2–22.8	–	–	–	[60]
	PD Patients (males or females ≥ 18 years old)	3–5 mg/kg	subcutaneous injection	6 (3 mg/kg); 10.3 (4 mg/kg); 12.4 (5 mg/kg)	0.3–0.4	1.0–1.2	7.4–16	7.4–16	–	–	98	
		3–5 mg/kg	subcutaneous apomorphine prefilled injection pen	7 (3 mg/kg); 11.5 (4 mg/kg); 16.8 (5 mg/kg)	0.3–0.4	0.8–1.0	8–16.7	8–16.7	–	–	83	
nuciferine	Healthy volunteers (18–45 years old, BMI = 19–24 kg/m <sup>2</sup> )	1.28–2.56 g Tangzhiqing tablet (nuciferine as its pharmacokinetics marker)	single-dose oral	1.6 (1.28 g); 2.1 (1.92 g); 3.8 (2.56 g)	1.8–2.0	1.3–1.6	5.3 (1.28 g); 7.4 (1.92 g); 13.3 (2.56 g)	5.4 (1.28 g); 7.5 (1.92 g); 13.3 (2.56 g)	–	–	–	[61]
		1.92 g Tangzhiqing tablet	oral 3 times/day for 6 days	2.4	1.6	1.9	9.3	10.5	–	–	–	
	SD rat (male, 250 ± 10 g)	28.8 mg/kg	Single dose oral	317.6	3.5	6.18	2069	2142	–	–	–	[64]
	SD rat (male, 250–300 g)	0.2 mg/kg	IV	–	–	0.6	119	119	1.8	1.5	–	[62]
		2–10 mg/kg	single dose oral	13.5 (2 mg/kg); 63.4 (5 mg/kg); 103 (10 mg/kg)	0.5–0.9	0.8–1.5	41.7 (2 mg/kg); 118.2 (5 mg/kg); 207.1 (10 mg/kg)	41.7 (2 mg/kg); 118.2 (5 mg/kg); 207.1 (10 mg/kg)	52.5–58.6	57.3–112.4	3.8–4.2	
		0.2 mg/kg	IV	–	–	6.6	2022.8	2026.3	0.3	0.9	1.9	[63]
		10 mg/kg	single dose oral	45.3	1	6.5	280.6	308.2	64.9	616.2	–	
	SD rat (male, 200 ± 20 g)	4.5 mg/kg	IV	–	0	2.09	2090	2130	2.2	9.5	58	[66]
		22.5 mg/kg	single dose oral	1710	0.9	2.48	6130	6200	2.2	7.9	–	
N-nuciferine	SD rat (male, 200 ± 20 g)	2 mg/kg	IV	–	0	3.84	7400	8500	2.6	15.2	80	[66]
		10 mg/kg	single dose oral	570	1.65	2.94	3320	3400	2.4	10.3	–	
O-nornuciferine	SD rat (male, 250 ± 10 g)	9.36 mg/kg	single dose oral with lotus extract	42.1	2.6	6.67	319.8	335.6	–	–	–	[64]
pronuciferine	SD rat (male, 250 ± 10 g)	9.41 mg/kg	single dose oral with lotus extract	210	4.9	4.44	2031	2096	–	–	–	[64]
liriodenine	SD rat (male, 250 ± 10 g)	3.6 mg/kg	single dose oral with lotus extract	54.7	5.7	3.77	415.1	429	–	–	–	[64]
magnoflorine	SD rat (male, 200 ± 20 g)	5 mg/kg	IV	2453.4	–	1.5	2430	2450.4	2.1	4.5	23	[72]
		15 mg/kg	single dose oral	181.5	–	13.2	1645.6	2384.9	8	122.9	–	
		10 mg/kg	IV	–	–	3.31	143.3	162.9	0.1	–	–	[142]
		10 mg/kg	IV	3948	–	1.27	2510	2517	4.1	7.5	–	[68]
		15 mg/kg	single dose oral	81.7	1.13	1.3	321.1	334.3	50.6	102.6	8.9	
		30 mg/kg	single dose oral	145.1	1.21	1.7	534.3	548	57.1	133.9	7.3	
		60 mg/kg	single dose oral	260	1.04	1.5	787.5	803.5	76.3	170.1	5.3	
		30 mg/kg	single dose oral with plant decoction	139.3	3	3.6	678.2	731.7	42.9	248.1	9.7	
	wistar rat (male, 260 ± 20 g)	6 mg/kg	IV	8517.80	0.1	0.66	2656	2674.70	2.3	–	3.7	[69]
		40 mg/kg	single dose oral	299.2	0.33	1.94	614.8	651.7	62.4	–	–	
	kunming mice (male and female)	12.02 mg/kg	single dose oral with plant decoction	–	–	–	1.4	–	–	–	–	[143]

(continued on next page)

Table 2 (continued)

Name	Model	Dose	Treatment	C <sub>max</sub> (ng/mL)	T <sub>max</sub> (h)	T <sub>1/2</sub> (h)	AUC <sub>0-t</sub> h*ng/mL	AUC <sub>0-∞</sub> h*ng/mL	CLL/kg/h	V <sub>d</sub> L/kg	F%	Ref
lauroitsine	rat (male, 200 ± 20 g)	2 mg/kg	IV	100.1	0.08	1.67	50	52.29	38.96	86	18	[86]
isoboldine	SD rat (male, 230 ± 10 g)	10 mg/kg	IV	14.1	0.47	3.73	40.6	47.77	218.26	1207.6	1.4	[85]
roemerine	SD rat (male, 200 ± 20 g)	30 mg/kg	IV	111	0.31	0.6	0.05	0.05	19.7	-	84	[41]
isocorydine	SD rat (male and female)	6 mg/kg	IV	1835	0	1.8	-	1631	3.8	9.4	84	[41]
		20 mg/kg	IV	1358	0.2	1.6	-	4541	4.4	10.2	34	[70]
		2 mg/kg	IV	1843.3	0.03	1.2	831.9	857.4	2.4	4.3	34	[70]
		20 mg/kg	IV	2496.8	0.3	0.9	2848.1	2865.3	7.2	9.3	34	[70]

6- OdemethylmenisporphineSD rat (male, 230 ± 10 g)0.1 mg/kg/singl e dose oral22012.85,121,21521,506---; not detected; PD: Parkinson's disease; IV: intravenous injection; C<sub>max</sub>: maximum plasma concentration; T<sub>max</sub>: time to reach C<sub>max</sub>; T<sub>1/2</sub>: terminal elimination half-life; CL: clearance rate, E<sub>body</sub> = CL/cardi ac output, above 0.35, around 0.15, around 0.05 was considered as high, medium and low elimination rate, respectively; V<sub>d</sub>: apparent volume of distribution; The oral absolute bioavailability: F(%) =  $\frac{AUC_{0-t}^{i.v.} \cdot Dose_{i.v.}}{AUC_{0-t}^{p.o.} \cdot Dose_{p.o.}}$  \* 100%; AUC<sub>0</sub>: the total area under the plasma concentration–time curve from 0 h to the last measured concentration, AUC<sub>∞</sub>: the area to infinite.

in clinical practice and *in vivo*. Among them, the clinical pharmacokinetics of apomorphine and nuciferine have been well studied. The concentration of alkaloids in different biological matrices, including plasma, tissues, urine, and feces, has been determined, and the pharmacokinetic parameters, as well as the metabolic pathways are summarized in Fig. 3, Table 2, and Table 3.

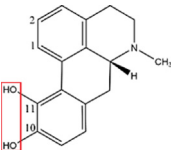
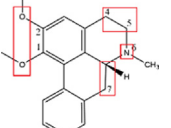
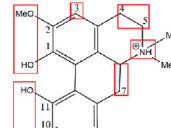
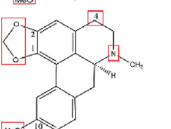
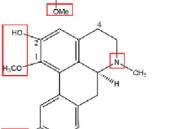
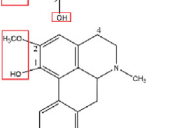
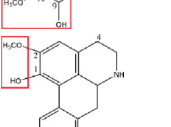
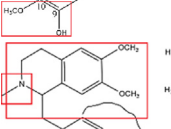
### Absorption

The absorption rate of AAs is highly associated with the maximum plasma concentration (C<sub>max</sub>) and time to reach the concentration peak (T<sub>max</sub>). The clinical absorption of apomorphine and nuciferine into the bloodstream is shown in Table 2. Clinically, the oral administration of apomorphine, a plant-derived AA generally used as an adjunctive medication in Parkinson's disease patients, was limited by its first-pass metabolism with low bioavailability (F%) < 4 % [60]. Therefore, the apomorphine sublingual film, subcutaneous apomorphine injection, and subcutaneous apomorphine prefilled injection pen were developed and showed high absorption rate in plasma, with C<sub>max</sub> > 10 ng/mL and T<sub>max</sub> < 0.8-h [60]. Subsequently, both the subcutaneous apomorphine injection (3, 4, 5 mg/kg with C<sub>max</sub> of 6, 10.3, and 12.4 ng/mL) and subcutaneous apomorphine prefilled injection pen (3, 4, and 5 mg/kg with C<sub>max</sub> of 7, 11.5, and 16.8 ng/mL) resulted in a dose-dependent systemic exposure (C<sub>max</sub>) and high oral absolute bioavailability (F value, 98 % and 83 %, respectively), while a low F value (17 %) was found using the sublingual film administration (Table 2), suggesting that the subcutaneous injection (SC) of apomorphine was more suitable for the clinical treatment [60]. Besides, nuciferine, as the pharmacokinetics marker of Tangzhiqing tablet used in patients, showed a dose-dependent blood absorption (1.28, 1.92, and 2.56 g Tangzhiqing tablet with C<sub>max</sub> of 1.6, 2.1, and 3.8 ng/mL) with T<sub>max</sub> < 2 h, which was attributed to its high permeable property [61].

Nuciferine used *in vivo* also exhibited rapidly absorption into the blood (T<sub>max</sub> < 1 h) and a dose-dependent systemic exposure. Nuciferine oral administration at the doses of 2, 5, 10, 22.5, and 22.8 mg/kg was rapidly distributed in the plasma, with a maximum concentration (13.5, 63.4, 103, 1710, and 317.6 mg/kg) after 0.9, 0.6, 0.5, 0.9, and 3.5 h, respectively, indicating the close association between absorption rate and administration dose (Table 2) [62–65]. The oral absolute F value of nuciferine was approximately 4 % with 10 mg/kg and 58 % with 22.5 mg/kg through oral administration [66], indicating that the F of nuciferine had dose-dependent effects. And the F value was increased by 3.3 ± 0.61-fold in nuciferine-loaded poly lactic-co-glycolic acid nanoparticles as compared to nuciferine alone [67]. Another two lotus alkaloids called N-nuciferine and roemerine were also rapidly absorbed into the blood and reached the C<sub>max</sub> (570 ng/mL and 1358 μg/mL, respectively) at 1.65 h and 0.22 h, with a good oral F value (79.9 %, and 84 %, respectively) [41,66].

The pharmacokinetics of magnoflorine, a naturally occurring simple AA, has been reported in many studies using rat and mouse models. Xue et al. [68] found that the F value of magnoflorine decreased from 8.9 % to 5.3 % as the concentration increased from 15 to 60 mg/kg, but subsequently increased to 9.7 % after the gavage of *coptidis rhizoma* decoction (equivalent to 30 mg/kg of magnoflorine), suggesting that the remaining substances of decoction performed a synergistic effect with magnoflorine absorption. Tian et al. [69] revealed that the coadministration of magnoflorine and berberine also enhanced the F value of magnoflorine. Besides, both simple aporphine isocorydine and oxoisoporphine 6-O-demethylmenisporphine underwent rapid (T<sub>max</sub> < 0.3 h and 3 h) and high absorption rate (F = 33.4 % and 51.5 %) after the administration of 20 mg/kg and 1 mg/kg, respectively, which was related to

**Table 3**  
Main metabolic pathways and related enzymes of natural aporphine alkaloids.

Natural Compound	Structure	Phase I reaction	Phase II reaction	Ref.
Apomorphine		Oxidation: OH → =O	Glucuronidation: 10- and 11-O-monoglucuronides O-methylation: OH → OCH <sub>3</sub> (COMT)	[76]
Nuciferine		N-oxidation: (CYP 3A4); Demethylation: OCH <sub>3</sub> → OH (CYP 1A2, 2A6, and 2C8) Dehydrogenation: C4-C5 and C6a-C7 (CYP 3A4) Hydroxylation: C5 → -OH (CYP 3A4)	N-glucuronidation (UGT1A4)	[65,144]
Magnoflorine		O-demethylation: 2,10-OMe N-demethylation Dehydrogenation: C4-C5 and C6a-C7, O-ketonization: 4-OH Hydroxylation: C-3, C-4, C-9	O-glucosylation, O-glucuronidation O-sulfation	[68]
Dicentrine		N-oxidation N or O, O-demethylation (1-OCH <sub>2</sub> O-2) Hydroxylation: C-3, C-4	Glucuronidation Glucosylation O-methylation: OH → OMe (C-4)	[82]
Boldine		N-demethylation (N-demethylboldine-O-sulphate)	Glucuronidation and Sulphation (boldine-O-glucuronide, boldine-O-sulphate and disulphate, boldine-O-glucuronide-O-sulphate)	[83]
Isoboldine		–	Glucuronidation Sulfonation: OH → SO <sub>3</sub> H	[85]
Norisoboldine		–	Glucuronidation: OH → GluA, Sulfonation: OH → SO <sub>3</sub> H (norisoboldine-1-O-β-d-glucuronide, norisoboldine-9O-α-d-glucuronide and disulfuric acid-1, 9-norisoboldine ester)	[84]
Thalicarpine		N-demethylation Aporphine ring oxidation Benzylic oxidation benzylic reduction	–	[87]

COMT: catechol-O-methyl transferase; CYP: Cytochrome P450 enzymes; UGT: UDP-glucuronosyltransferases.

their small molecular weight ( $M_w$  < 400), high lipophilicity and permeability [70,71].

### Distribution

Clinically, apomorphine quickly crossed the blood–brain barrier (BBB) and both enantiomers of apomorphine equally and uniformly concentrated in different brain tissues, showing neurotropic properties. Moreover, apomorphine quickly crossed the nasal and intestinal mucosa, thus nasal and rectal administration were used for disease treatment [60].

The distribution of AAs was highly associated with apparent volume of distribution ( $V_d$ ). A wide tissue distribution of nuciferine has been found *in vivo*, with a  $V_d > 50$  L/kg, mainly accumulated in the kidney and lung, followed by spleen, liver, brain, heart, and adipose tissue after oral administration, and similar distribution of N-

nuciferine and roemerine has been found [41,62,63,65,66]. The high concentration in the lung, kidney, and spleen was possibly attributed to the high blood flow in these organs, and the presence of nuciferine in the liver and adipose tissue provided a proof for its anti-obesity and hypolipidemic effects [62]. The low  $F$ -value and high accumulation of nuciferine in the kidney may be an obstacle to developing an oral formulation for long-term use, as it presents a potential risk of kidney toxicity.

Magnoflorine, generally isolated from the herbal medicine *Coptis chinensis* Franch., was widely distributed in the liver, followed by spleen and lung, and the lowest in the brain [72]. The significant difference of  $V_d$  values observed in the oral administration of the *Coptis* rhizoma decoction ( $V_d = 248.1$  L/kg) and magnoflorine alone ( $V_d = 102.6$ – $170.1$  L/kg) highlighted the importance of considering the co-treatment of magnoflorine with other phytochemicals for human health [68].

Taspine was generally used to enhance wound healing and both taspine solution and taspine liposome demonstrated a wide distribution in the liver, spleen, lung, kidney, heart, and penetrate through the BBB. The administration through liposome obviously prolonged the residence time in the systemic circulation, increased the liver concentration, and decreased the heart accumulation [73]. 6-O-demethylmenisporphine, an oxoisoAA extracted from *Menispermis Rhizoma*, was also widely distributed in the kidney, heart, lung, liver, muscles, spleen, and brain. According to experimental data from urine, bile, and feces, the prototype drug (6-Odemethylmenisporphine) was completely excreted at 24, 24, and 12 h, respectively, suggesting that it was widely metabolized *in vivo* and the metabolites were subsequently eliminated [71].

The permeability of compounds from the blood system to the tissues for their distribution is determined by their physicochemical properties, especially liposolubility. The brain distribution of AAs also plays an important role in the regulation of the central nervous system. Apomorphine, nuciferine, N-nuciferine, and roemerine rapidly crossed the BBB due to the simple diffusion related to the high lipophilicity at physiological pH, contributing to exert sedative-hypnotic and anxiolytic effects in the brain [66]. Besides, effective apomorphine-loaded nanoparticles have been designed for improving the brain accumulation of apomorphine [74]. The similar structure between isocorydine and apomorphine indicated that isocorydine effectively crossed the BBB, implying its central pharmacological activity [70]. 6-Odemethylmenisporphine exerted a potential therapeutic effect on nervous disorders by enhancing the cholinergic neurotransmission and reducing acetylcholinesterase aggregation [71]. Due to its weak neuroregulatory effect, alternative strategies are required to enhance the liposolubility and permeability of magnoflorine, ultimately improving its neuroprotective activity [75].

### Metabolism

AAs are catalyzed by various enzymes in the body, especially cytochrome P450 (CYP) and uridine diphosphate glycosyltransferase (UGT), and participate in multiple chemical reactions in the metabolic process, which commonly include two steps (Fig. 3). On the first step, oxidation, reduction, and hydrolysis reactions introduce polar groups (for example –OH, –SH, and –NH<sub>2</sub>) to the functional groups for enhancing the water solubility of metabolites. On the second step, the obtained metabolites are bound to endogenous substances to produce more hydrophilic compounds, further excreted through the kidney, intestine, and other ways. Table 3 shows the metabolic pathways of AAs.

Apomorphine was easily and mainly (auto)oxidized, followed by glucuronidation and sulfation in patients with Parkinson's disease [76]. The phase II metabolites were 10- and 11-O-monoglucuronides as well as apocodeine, and a small amount of isoapocodeine was generated through the catechol-O-methyl transferase, as shown in Table 3. Traditional Chinese Medicine K-601 has been studied in pharmacokinetics research involving six healthy males. Magnoflorine, one of the major compounds in K-601, underwent primarily phase I metabolism (specifically demethylation) and phase II metabolism (including glucuronidation, acetylation and sulphation) [77]. Similar results were found in both *in vivo* and *in vitro* studies, showing that 12 metabolites of magnoflorine have been detected (8 phase I metabolites originated from N or O-demethylation, O-ketonization, dehydrogenation and hydroxylation and 4 phase II metabolites originated from O-glucosylation, O-glucuronidation and O-sulfation) (shown in Table 3) [68]. Gut microbiota and their metabolites enzymatically transform natural products to affect compounds pharmacokinetics and bioavailability profiles. Phase I biotransformation of magnoflorine is activated by anaerobically incubation mag-

noflorine with gut microbiota (the supernatant of rats' fresh feces) *in vitro* [68].

A comprehensive metabolic generation mechanism of nuciferine was elaborated *in vivo*. 55 metabolites were identified from mice, involving 29 phase I metabolites and 26 phase II metabolites [78]. To further examine the metabolic mechanism of nuciferine, the enzymes' catalytic activities were evaluated *in vitro* incubation systems. As shown in Table 3, the main phase I enzymes including CYP1A2, CYP2A6, CYP2C8 for demethylation, and CYP3A4 for N-oxidation, dehydrogenation and hydroxylation, and the phase II enzymes including UGT1A4 and UGT1A9 for N-glucuronidation, as well as the sulfated-related enzymes SULT1A1''1 and SULT1A1''2 confirmed high catalytic activities for metabolites formation of nuciferine [78,79]. The molecular docking analysis was also identified the interaction between nuciferine and CYP isoforms [78]. Although nuciferine is catalyzed by many enzymes, it competitively inhibited CYP2D6 activity with N-nornuciferine and 2-hydroxy-1-methoxyaporphine due to their aporphine parent nucleus, resulting in potential adverse drug interactions in the clinic, which should be further studied [80]. Meanwhile, the gut microbiota *Akkermansia*, *Lactobacillus*, and *Bifidobacterium* were possibly involved in the metabolism of nuciferine in gestational diabetes mellitus mice, but the understanding of how gut microbiota directly and indirectly affect AAs metabolism is limited studied [81].

Table 3 showed that the metabolic profile of dicentrine, a simple AA rich in a variety of genera in the plant family Lauraceae, consists of 24 metabolites characterized in pig urine, including 9 phase I and 15 phase II conjugates, and the phenolic group of dicentrine underwent glucuronidation and glucosylation while no sulfation was observed after phase I biotransformation [82]. As one of the simple aporphines and most potent natural free radical scavengers, boldine was identified as the main compound biotransformed through N-demethylation in phase I and subsequently through O-conjugation with glucuronic and sulphuric acid in phase II [83]. The free hydroxyl groups in the boldine were directly available for conjugation and they were beneficial for performing phase II bio-transformation.

Boldine, isoboldine, and norisoboldine have a similar structure, implying the similar pharmacokinetic and metabolic profiles in rat plasma, bile, urine and feces, such as the common glucuronidation and sulphation in phase II bio-transformation [84,85]. Therefore, a reasonable hypothesis was proposed that isoboldine and norisoboldine may also undergo N-demethylation during their phase I metabolism. As shown in Table 3, the major glucuronidation and sulphation generally occurred on –OH group of three AAs. The mentioned metabolic pathways may also be suitable for laurolsine due to a similar structure of laurolsine with isoboldine [86]. Thallicarpine, a dimeric AA consisting of aporphine and benzyltetrahydroisoquinoline units, was metabolized through three pathways, such as N-demethylation, aporphine ring oxidation, and benzylic oxidation/reduction (phase I). Only one metabolite was identified as glaziovine glucuronide found in urine samples [87].

In summary, it is likely that most AAs shared common characteristics such as the high absorption (generally C<sub>max</sub> > 10 ng/L, T<sub>max</sub> < 3 h) and elimination (generally T<sub>1/2</sub> < 3 h, CL > 50 L/kg/h) rate, and the nonspecific biodistribution, which can be attributed to their small molecular weight, nonpolar hydrocarbon backbones and hydrophobic functional groups like aromatic rings. The liver and the gut play an important role in drug metabolism, including methylation, N- or O-demethylation, O, O-demethylation, N-oxidation and reduction for phase I metabolic transformation, and N- or O-glucuronidation, O-glucosylation, sulphation, and sulfonation for phase II metabolic transformation, which was regulated by CYP and UGT enzymes. Similar metabolites were found

in both *in vivo* bio-samples and *in vitro* incubation systems of AAs and gut microbiota during AAs metabolism, suggesting a potential influence of gut microbiota on this process. However, as the metabolic effects of the gut microbiota are rarely studied in AAs pharmacokinetic research, the contribution of the gut microbiota to AAs metabolism is probably underestimated. Additionally, while most studies are now characterizing the metabolites derived from biotransformation of AAs, these data remain pre-clinical in nature, and more clinically actionable insights in specific pharmacokinetic parameters of AAs should be reported in future.

## Safety

The toxicities of AAs are tightly linked with the dosage and administration methods, such as oral, SC, and intraperitoneal injection (IP). A mixture of Chinese herbal medicines containing nuciferine (0.9 mg/g), nornuciferine (0.3–0.4 mg/g), and O-nornuciferine (0.3 mg/g) was administered under the oral treatment of 4.38 g/day Hedan Tablets to patients with hyperlipidemia for 8 weeks. The levels of the proprotein convertase subtilisin/kexin type 9 (a circulating protein that is negatively correlated with drug efficacy) were not altered, and no change was also found in the levels of alanine aminotransferase and aspartate aminotransferase, indicating the Hedan Tablets exert beneficial effects without evident toxicities [88]. The subacute toxicity test confirmed the safety of magnoflorine in a certain dose range in mice. No evident toxicity was observed after 4 weeks of continuous intragastric administration at a dose of 100 mg/kg and 200 mg/kg. No significant reaction was observed after the administration of 40 mg/kg magnoflorine by gavage in cats for 4 h.

The most common administration route for apomorphine is SC due to its low bioavailability (<4%) in oral therapy. The primary administration route in Parkinson's disease includes continuous subcutaneous apomorphine infusion and intermittent injections. The usual dose of apomorphine in patients was 2–6 mg/kg, with a total of 88 mg (range 24–340 mg) as daily clinical application [89]. The adverse event rate of continuous subcutaneous apomorphine infusion, which reduced the duration (–50 %) and the severity (–45 %) of the dyskinesias, was usually lower than that after intermittent injections, promoting the duration (+33 %) and the severity (+14 %) of the dyskinesias [90]. The most widespread side effects were subcutaneous nodules, nausea, and somnolence. Apomorphine therapy caused infrequent immune hemolytic hematologic anemia at the dose of 75 mg/d [91]. Other ways of apomorphine administration include buccal, inhalation, and pump-patch routes, which were promising delivery strategies as a substitution therapy for patients with needle phobia [60].

An IP of 50 mg/kg magnoflorine in mice significantly increased the plasma levels of IL-6 and IL-1 $\beta$ , and exerted a negative effect on neuronal Ca<sup>2+</sup> metabolism, subsequently leading to neurotransmission disorders. On the contrary, no significant changes were observed in the levels of interleukin (IL) 1 $\beta$ , IL-6 or tumor necrosis factor  $\alpha$  (TNF- $\alpha$ ) after a low dosage through IP of magnoflorine (10 and 20 mg/kg) [92]. The median lethal dose of N-nornuciferine with lower levels of hyperlipemia and cholesterol, was 323  $\mu$ g/kg (IP) in mice [93]. Boldine, administered at a dose of 100 mg/kg through IP to rats for 14 days, resulted in no mortality or any onset of clinical or toxicological symptoms throughout the study period [94].

The toxicity of AAs has been studied on normal cell lines *in vitro* as well. The cytotoxicity of oxoglucine, an oxoaporphines originated from herbal medicine, against two human normal cell lines HL-7702 and HUVEC was 40.2  $\pm$  1.0  $\mu$ M (IC<sub>50</sub>) and 90.2  $\pm$  1.3  $\mu$ M (IC<sub>50</sub>), respectively, indicating its low toxicity [95]. Besides, two dehydroAAs isolated from the roots of *Thalictrum foetidum*, such

as 9-(2'-formyl-5',6'-dimethoxyphenoxy)-1,2,3,10-tetramethoxy dehydroaporphine and 9-(2'-formyl-5', 6'-dimethoxyphenoxy)-1, 2, 3, 10-tetramethoxy oxoaporphine, exhibited an antitumor effect against glioblastoma stem cells 3 times higher than that on the human normal cell line (293 T, IC<sub>50</sub> = 15.5 and 8.2  $\mu$ g/mL, respectively), suggesting its significant selective cytotoxic effect on different cells [93]. Toxicity studies suggested that most AAs had non-toxic or low-toxicity properties. However, long-term and high-dose safety tests in clinical practice are still lacking.

## Anticancer activities of AAs on cancer

Anti-cancer effects of AAs on multiple cancer types, including hepatocellular carcinoma, gastric, colorectal, pancreatic, and lung cancer, have been widely studied (Table 4). Although few clinic trials are reported so far, abundant evidence shows significant anti-cancer effect after a treatment with AAs alone or a synergistic treatment with metal/clinical therapeutic drugs.

### Anti-cancer effect of AA alone

Nuciferine, the main simple AA present in lotus leaf, was used in a murine subcutaneous transplantation model with colorectal carcinoma CT26 cells and SY5Y cells at a dose of 9.5 mg/kg, IP, and the results show that the tumor weight is significantly smaller than that of the control group. Notably, the anticancer activity in the group of mice treated with nuciferine soon after tumor implantation is higher than that in the mice treated with nuciferine when the tumor reached a size of 100 mm<sup>3</sup>. [96] Nuciferine (50 mg/kg, IP) in the presence of nicotine significantly inhibits tumor weight and size in the murine subcutaneous transplantation model with lung adenocarcinoma A549 cells, virtually eliminating the proliferative effect of nicotine in non-small cell lung cancer [97]. Nuciferine significantly inhibits laryngeal squamous cell carcinoma survival in a concentration-dependent manner by inhibiting the *Tripartite Motif Containing 44* mRNA levels and inhibiting the activation of Toll-like receptor 4 (TLR4) downstream kinases such as protein kinase B (AKT) signaling pathway, which is detected in the murine subcutaneous transplantation model with laryngeal squamous cell carcinoma TU212 cells [98]. The effect of 1 mg/mL nuciferine treatment at an early stage of carcinogenesis is superior to that at a middle stage in the murine subcutaneous transplantation model with neuroblastoma SY5Y cells [96]. In the transplantation model with glioblastoma U251 cells, the tumor weight and size of the 15 mg/kg nuciferine-treated group is significantly smaller than those in the control group, and tumor progression markers Ki67, CDC2, Bcl-2, HIF1 $\alpha$ , and N-cadherin are decreased in the nuciferine-treated group [75].

The antitumor effect of isocorydine, a simple aporphine with a 5, 6, 6a, 7-tetrahydro-4H-dibenzo quinoline core, was studied in a liver cancer model induced using hepatocellular carcinoma side population cells. The treatment with isocorydine (0.4 mg/kg) significantly reduces tumor weight by 50 % compared to that of the vehicle group in side population cell-induced mice, whereas no significant difference in tumor size and tumor weight is found between isocorydine and vehicle treatment in the non-side population group, indicating that isocorydine selectively inhibits the growth of side population cells [99]. The results are confirmed by a murine subcutaneous transplantation model of hepatoma using hepatocellular carcinoma Huh7 or SMMC-7721 cells [100].

Boldine, isolated from the bark and leaves of the Boldo tree (*Peumus boldus*), also shows excellent antiproliferative and apoptotic properties on cancer cells. Oral supplementation with boldine (90 mg/kg) in diethylnitrosamine induced rats of liver cancer significantly decreases liver weight as well as the serum tumor mark-

**Table 4**  
Anticancer activities of aporphine alkaloids on various cancer types.

	Cancer type	Constituents	Model/Cell (IC <sub>50</sub> )	Dose	Effects	Mechanisms	Ref	
<i>In vivo</i>	Hepatocellular carcinoma	Isocorydine	Murine Model with SP cells from MHCC-97L cells	0.4 mg/kg (IP)	↓Tumor volume; ↓Tumor weight	↑Fas; ↑Bax; ↑Bim; ↑Bik; ↑Bak; ↑puma; ↓Bcl-2; ↓Bcl-xl; ↓Mcl-1	[99]	
		Isocorydine	Murine Model with Huh7 or SMMC-7721 cells	0.4 mg/kg (IP)	↓Tumor volume; ↓Tumor weight	↑p-Chk1; ↑p-Chk2	[119]	
		8-acetamino-isocorydine	Murine Model with H22 cells	100 mg/kg (oral)	↓Tumor volume; ↓Tumor weight	–	[35]	
		8-amino- isocorydine	Murine model with HCC-LY5 cells	0.12 mg/mice (IP)	↓Tumor weights; ↓Tumor volumes	↑C/EBPβ	[100]	
		Boldine	Rats model treated by diethylnitrosamine	90 mg/kg (oral)	↑Liver weight	↓Bcl2; ↑Bax; ↑cytochrome c; ↑cleaved caspase 3	[94]	
	Colorectal cancer	Oxoglucine	Murine model of hepatoma with BEL-7402 cells	75 mg/kg (IP)	↑Tumor growth inhibition rate	–	[95]	
		Chiral platinum (II)-4-(2,3-dihydroxypropyl)-formamide	Murine model with BEL-7404 and BEL-7402 cells	8 mg/kg (IP)	↓Tumor growth	↓hTERT; ↓ c-myc	[103]	
		oxoaporphine	Murine model with BEL-7402 and T-24 cells	5 mg/kg (IP)	↓Tumor growth	↑ROS; ↑Apaf-1; ↑cytochrome c; ↑caspase-3/9	[145]	
		cobalt oxoisoaporphine complexes	Murine model with HepG2 cells	6 mg/kg (IP)	↓Tumor weights; ↓Tumor volumes	↑p53; ↑p21; ↑p27; ↑Chk1; ↑Chk2	[105]	
		Oxoaporphine-Zn complexes	Murine model with SGC7901 cells	10 mg/kg (IP)	↓Tumor cell density	↓AKT; ↓JNK	[110]	
		Magnoflorine	Murine model with CT26 cells and SY5Y cells	1 mg/mL (IP)	↓Tumor weights	↑PI3K-AKT and IL-1β levels	[96]	
		Nuciferine	Murine model with NCI-H460 cells	6 mg/kg (IP)	↓Tumor weights; ↓ volumes	↑Caspase-3/9; ↓Telomerase	[104]	
		Organoplatinum (II) complexes with Oxoisoaporphine						
		Isocorydine	murine model with PANC-1 cells	0.4 mg/kg (IP)	↓Tumor weights; ↓Tumor volumes	↓p-STAT3	[106]	
		Nuciferine	Murine model with PANC-1 cells	30 mg/kg (IP)	↓Tumor volume; ↓Tumor weight	↓pYAP	[107]	
		Lung cancer	Nuciferine	Murine model with A549 cells	50 mg/kg (IP)	↓Tumor weight; ↓Tumor size	↑Axin; ↑Bax; ↓β-catenin; ↓Bcl-2	[97]
			Nuciferine	Murine model with LA795 cells	30 μM (oral)	↓Tumor growth	↑TMEM16A	[2]
		Glioblastoma	Nuciferine	Murine model with A549/T cells	7.5 mg/kg (IP)	↓Tumor growth; ↓Tumor size	↓PI3K/AKT	[108]
			Nuciferine	Murine model with U251 cells	15 mg/kg (IP)	↓Tumor size, ↓angiogenesis; ↓hardness index	↓p-AKT; ↓p-STAT3; ↓SOX2	[120]
Breast cancer	Boldine	Rat model with LA7 cells.	100 mg/kg (IP)	↓Tumor growth	↑caspase-3/7; ↓NF-κB	[111,114]		
	KO-202125	Murine model with MDA-MB-231 cells	1.95 mg/kg (oral)	↓Tumor growth	↓AKT	[111]		
	Magnoflorine	Murine model with MCF-7 cells.	3 mg/kg (IP)	↓Tumor volume; ↓Tumor weight	↑caspase-3; ↑LC3-II; ↑p-p38	[20]		
	7-hydroxydehydronuciferine	Murine model with A375.S2 cells	20 mg/kg (IP)	↓Tumor size	↑PI3k/AKT	[121]		
	Apomorphine	Zebrafish transgenic model	50 μM	↓Vascular formation	–	[19]		
<i>In vitro</i>	Hepatocellular carcinoma	Magnoflorine	HepG-2 (0.4 μg/mL)U251 (7 μg/mL)	1–10 μg/mL	↓Cell viability	–	[39]	
		Lanuginosine	HepG-2 (2.5 μg/mL)U251 (4 μg/mL)	1–10 μg/mL				
	Colorectal cancer	Xylopinine	HepG-2 (6.31 μM)	5, 10 μg/mL	↑Cytotoxicity	↑G2/M arrest	[101]	
		Xylopinine	HepG-2 (9.4 μM)	14 μM	↑Cytotoxicity	↑G2/M phase arrest; ↑p53-independent pathway	[122]	
		Boldine	HepG-2 (55.66 ± 1.3 μM)	50 μg/mL	↓Cell viability	↑G2/M arrest, ↑caspase-9 and caspase-3/7	[125]	
		8-hydroxyartabonatin C	HepG-2 (12.9 μM)	60 μM	↑Cytotoxicity	–	[135]	
		ouregidione	HepG-2 (26.3 μM)	60 μM	↑Cytotoxicity	–		
		Platinum (II) complex of Liriodenine	BEL-7404 (6.9 μM)	10 μM	↓Cell proliferation	↑S/G2/M phase arrest; ↓Telomerase	[103]	
		7-hydroxydehydronuciferine	AGS (62.9 μM)	100 μM	↓Cell proliferation	–	[41]	
		Xylopinine	HCT-116 (6.4 μM)	14 μM	↑Cytotoxicity	G2/M phase arrest; ↑p53-independent pathway	[122]	
		D-dicentrine analogues	COLO 201 (3.9 μM)	10 μM	↑Apoptosis	↑TOP2; ↑G2/M arrest	[146]	
		Lung cancer	Crebanine	A549 (25 μg/mL)	5–15 μg/mL	↓Proliferation; ↓Migration	↑TNF-α; ↓NF-κB; ↓Bcl-2	[147]
	Thailandine		A549 (0.30 μg/mL)	50 μg/mL	↑Cytotoxicity	–	[139]	
	Laryngeal Squamous Cell Carcinoma	Magnoflorine with cisplatin	NCIH-1277 (36.5 μg/mL)	–	↓Proliferation; ↓Migration	↑p53; ↑caspase-3; ↑LC3-II; ↑p-p38; ↓p-AKT	[118]	
		Xylopinine	SCC9 (26.6 μM); HSC3 (15.7 μM)	14 μM	↑Cytotoxicity	G2/M phase arrest; ↑ p53-independent pathway	[122]	
	Glioblastoma	Magnoflorine	U251 (7 μg/mL)	1.1 mg/mL	↓Cell viability	–	[39]	
		lanuginosine	U251 (4 μg/mL)	1.1 mg/mL	↓Cell viability	–		
	Breast cancer	AAs isolated from <i>Thalictrum foetidum</i>	GSC-3 <sup>#</sup> , GSC-18 <sup>#</sup> (2.36–5.37 μg/mL)	0.5–60 μg/mL	↓Cell viability	–	[93]	
		Boldine	MCF-7 (160 μM)	63–2000 μM	↓Proliferation	↓Telomerase	[125]	
		N-benzylsecoboldine	MCF7(16.25 μM); MDA-MB-231 (21.88 μM)	–	↓Cell viability	↓Telomerase	[124]	
Crebanine		MCF-7 cells (27 μg/mL)MDA-MB231 (15 μg/mL)	5–15 μg/mL	↓Cell viability	↑TNF-α; ↓NF-κB; ↓Bcl-2	[147]		
Oxocrebaine		MCF-7 (16.66 μM)	4–64 μmol/L	↓Proliferation; ↓migration	↑DNA damage; ↑Autophagy	[126]		
Four AAs isolated from <i>Stephania venosa Spreng</i>	MDA-MB231 (4–40 μg/mL)	1 mg/mL	↓Proliferation	↑G2/M arrest; ↑Apoptosis	[139]			

Table 4 (continued)

Cancer type	Constituents	Model/Cell (IC <sub>50</sub> )	Dose	Effects	Mechanisms	Ref
	Two AAs isolated from <i>Fissistigma glaucescens</i>	MCF-7 (3.2–8.1 μg/mL)	–	↑Cytotoxicity	–	[43]
	Xylophine	MCF-7 (12 μM)	14 μM	↑Cytotoxicity	↓G2/M phase arrest; ↑ p53-independent pathway	[122]
Melanoma	Four AAs isolated from <i>Stephania venosa</i> Spreng	MCF-7 (22.2 μM; 23.9 μM)	1 mg/mL	↑Cytotoxicity	–	[139]
	N-methylasimilobine(-)-liridinine2-hydroxy-1-methoxy-6a,7-dehydroaporphine	Melanogenesis 4A5 cells (15.8 μM; 14.5 μM; 19.3 μM; 13.3 μM)	3–30 μM	↓Melanogenesis	↓Tyrosinase; ↓TRP-1; ↓TRP-2	[42]
Epithelial ovarian cancer Osteoma cells Leukemia	Liriodenine	CAOV-3 (37.3 μM)	20–40 μM	↓Cell viability	↑S phase arrest; ↑caspase-3; ↑caspase-9	[25]
	Magnoflorine with cisplatin Xylophine	MG-63 (2.05 μM); U-2 osteoma (4.81 μM) HL-60 (18.5 μM)/K562 (7.8 μM)	– 14 μM 14 μM	↓Proliferation; ↑Invasion ↑Cytotoxicity	↑HMGB1; ↑NF-κB; ↑miR-410-3p ↓G2/M phase arrest; ↑ p53-independent pathway	[118] [122]

AKT: protein kinase B; AMPK: AMP-activated protein kinase; Apaf-1: the apoptotic protease activating factor-1; CDK1/2: cyclin dependent kinases 1/2; hTERT: human telomerase reverse transcriptase; IP: intraperitoneal injection; IL: interleukin; JNK: stress-activated protein kinases; NF-κB: nuclear factor κB; PI3K: phosphatidylinositol 3-kinase; ROS: reactive oxygen species; STAT3: activator of transcription 3; SOX2: sex determining region Y (SRY)-box 2; TNF-α: tumor necrosis factor α; TMEM16A: the transmembrane protein 16A; YAP: YES-associated protein Ser127.

ers alpha-fetoprotein and carcinogen embryonic antigen [94]. The oxoaporphine 7-hydroxydehydroneuciferine inhibits malignant melanoma in mice subcutaneously transplanted with melanoma A375.S2 cells.

AAs inhibit cancer cell growth *in vitro*. Magnoflorine and lanuginosine, which were separated from the methanol extract of magnolia leaves, exert a significant cytotoxicity on HEPG2 cells, with an IC<sub>50</sub> value of 0.4 and 2.5 μg/mL, respectively [39]. Nineteen alkaloids were isolated from the stem of *Xylopija laevigata*, and most of these alkaloids exert a significant cytotoxicity against HepG2 cells, with IC<sub>50</sub> values below 15 μg/mL, indicating the high inhibition rate. Remarkably, (+)-xylophine shows the strongest cytotoxic activity, with a IC<sub>50</sub> value of 1.87 μg/mL in HepG2 cells [101]. Most of the studies are based on the separation and purification of aporphines followed by cancer inhibition experiments without further confirmation *in vivo* studies. The specific AAs tested *in vivo* and *in vitro* are listed in Table 4.

#### Structure-anticancer activity relationship: Role of the C8 position of AAs

Previous studies showed that AAs possess a relatively planar conformation, readily inserted into the DNA double helix, promoting DNA sequence changes, stimulating DNA strand breaks, or inhibiting DNA topoisomerase II activity [102]. The target modified product is 8-amino-isocorydine, which is obtained by the replacement of an amide group at C8 on simple AAs to maintain the more stable planar conjugate configuration, further modified as 8-acetamino-isocorydine due to its instability in aqueous solution. The prodrug 8-amino-isocorydine (100 mg/kg) has a significant antitumor activity by reducing tumor weight by 53.12 % in the murine transplantation model with hepatocellular carcinoma H22 cells. Although the inhibitory effect of 100 mg/kg 8-amino-isocorydine is not stronger than cyclophosphamide used as the positive group, the average body weight of the cyclophosphamide group is significantly lower than that of the isocorydine group and control group, suggesting its dangerous potential effect in clinical practice.

Besides, a nitric acid group and a weak electron-donating group were introduced at the C8 position. The compound with a strong electron-donating group (-NH<sub>2</sub>) at the C8 position has better anticancer activity than the compound with an electron-withdrawing group (NO<sub>2</sub>) and a weak electron-donating group at the C8 position [35]. The 8-amino-isocorydine is obtained after reduction of the amide group at C8, which shows inhibitory effect on tumor size in hepatocellular carcinoma mice. The treatment with 0.12 mg/kg 8-amino-isocorydine has similar effects compared to those of 0.2 mg/mouse sorafenib treatment, which is used in clinical practice in liver cancer patients, in the murine subcutaneous transplantation model with hepatocellular carcinoma HCC-LY5 cells [100]. A Treatment with 250 mg/kg/8-amino-isocorydine significantly reduces the size and weight of tumors better than that of 40 mg/kg 5-FU in murine subcutaneous transplantation model with gastric cancer MGC803 cells. Moreover, the body weight is not different from that of the control group, indicating the low toxic effect of 8-amino-isocorydine. These results indicate the important role of the C8 position of aporphines, which may be a target position for drug design and synthesis.

#### Synergistic anticancer bioactivities

**Synergy with metals.** Since the successful application of platinum-based anticancer drugs, anticancer metal complexes have attracted great interest. Oxoaporphine and oxoisoAAs isolated from traditional Chinese medicines possess antitumor activity, so these two kinds of aporphines are used as ligands. Over the

last decades, platinum (II)-based drugs have been widely used in anticancer chemotherapies. However, they inevitably induce drug resistance, serious side effects, and they are highly toxic. The tumor inhibition rate of the 8 mg/kg chiral platinum (II)-4-(2,3-dihydroxypropyl)-formamide oxo-aporphine complexes used in the murine subcutaneous transplantation model with hepatocellular carcinoma BEL-7404 cells and BEL-7404 cells, reached 46.8 % and 47.1 %, respectively [103]. The organoplatinum (II) complexes with Oxoisoaporphine (Pt2) (6 mg/kg) treatment results in a dose-dependent inhibition of tumor growth with an inhibition rate of 38.5 % and less toxicity than cisplatin in a lung cancer mouse transplantation model [104].

Cobalt, one of the main trace elements in cells, shows anticancer effects. The therapeutic effect of 5 mg/kg cobalt oxoisoaporphine complexes in the murine subcutaneous transplantation model with hepatocellular carcinoma BEL-7402 and T-24 cells is similar to that of cisplatin treatment, with an inhibition ratio of 65.7 %. Zn (II) complexes are synthesized by oxoaporphine derivative (0.03 mmol, 0.0109 g), methanol (1.5 mL), and chloroform (0.5 mL). A total of 6.0 mg/kg oxoaporphine-Zn to the murine subcutaneous transplantation model with hepatocellular carcinoma HepG2 cells is able to control tumor growth with a volume reduction of 55.57 %, and a tumor weight inhibition rate of 32.8 % [105]. It is worth noting that the above-mentioned complexes have a much lower body weight inhibition rate than the drug cisplatin used as a positive sample, indicating a lower toxicity *in vivo*.

**Synergy with clinical therapeutic drugs.** AAs have synergistic effects with drugs, reducing drug resistance or increasing sensitization. Gemcitabine is widely considered as a preferential treatment option for locally advanced and metastatic pancreatic cancer. Isocorydine reduces the expression of p-signal transducer and activator of transcription 3 (STAT3) in pancreatic cancer cells induced by gemcitabine, down-regulates the expression of transcription factors and proteins related to epithelial-to-mesenchymal transition (EMT), and inhibits the migration and invasion of tumor cells. The combination of isocorydine (0.4 mg/kg) and gemcitabine (100 mg/kg) significantly inhibits tumor growth in the murine subcutaneous transplantation model with pancreatic cancer PANC-1 cells, with a significantly greater effect than isocorydine or gemcitabine alone [106]. Nuciferine has also anticancer activity when used in synergy with gemcitabine, and it significantly reduces the resistance to gemcitabine. Nuciferine (30 mg/kg) in the murine transplantation model with pancreatic cancer PANC-1 cells reduces the resistance to 20 mg/kg gemcitabine by activating the AMP-activated protein kinase (AMPK)-mediated down-regulation of 3-hydroxy-3-methyl-glutaryl-coA reductase (HMGCR) in pancreatic cancer cells associated with an increase in YES-associated protein Ser127 (YAP) phosphorylation [107].

Although cisplatin is frequently used in the clinical treatment of lung cancer, high dosage is associated with a strong toxicity. The tumor size of a murine subcutaneous transplantation model with lung adenocarcinoma LA795 cells treated with 30  $\mu$ M nuciferine is significantly reduced, with an inhibition rate of 40.1 %. Notably, the cotreatment of nuciferine (30  $\mu$ M) and cisplatin significantly increases the tumor inhibition rate (15 mg/kg, 80.4 %), which is higher than that of the treatment of cisplatin alone (15 mg/kg, 72.9 %) [2]. Besides, the resistance to the drug paclitaxel, doxorubicin, docetaxel and daunorubicin in A549/T and HCT-8/T cell lines is reduced by the combination therapy with nuciferine. The inhibition of the phosphatidylinositol 3-kinase (PI3K)/AKT/ extracellular signal-regulated kinases (ERK) pathway, the activation of the nuclear factor E2-related factor 2 (Nrf2) and hypoxia-inducible factor-1 $\alpha$  (HIF-1 $\alpha$ ), and the decrease of the expression of P-glycoprotein (P-gp) and breast cancer resistant protein (BCRP) may contribute to the sensitization of nuciferine to multidrug resistance in various cancers [108]. A stronger tumor suppression

effect is associated to the cotreatment of doxorubicin (3 mg/kg) and magnoflorine (3 mg/kg) compared with the effect of doxorubicin (3 mg/kg) alone, achieved by the regulation of the AKT/mechanistic target of rapamycin (mTOR) and p38 signaling pathways. Notably, magnoflorine alone has no significant anticancer activity and no evident toxicity *in vivo*, suggesting that magnoflorine has the potential to be used as a sensitizer of doxorubicin in clinical practice [20].

#### Strategies of AA-delivery system for application

Designation of AAs-loaded nanoparticles as carriers to improve the pharmacological activities of AAs in food and medicine application has paid attention over the last two decades. For example, the nuciferine-loaded poly lactic-co-glycolic acid nanoparticles were constructed for sustainable targeted release of nuciferine. Compared with free nuciferine, the nuciferine-loaded nanoparticles significantly decreased the levels of serum total cholesterol, triglycerides and low-density lipoprotein cholesterol and increased high-density lipoprotein cholesterol, which exhibited improvement of potential bioactivities against hepatocarcinogenesis on high-fat diet-induced hyperlipidemia rat [67]. The magnoflorine-loaded chitosan collagen nanocapsules significantly decrease the level of pro-inflammatory cytokines, including IL-1 $\beta$ , IL-6, and TNF- $\alpha$ , more than free magnoflorine administration in cognitive deficit rats, indicating a great role of nanocapsules on magnoflorine delivery and enhancement of bioactivities against inflammation-driven cancer progression [109].

#### Mechanism of action of AAs against cancer

The mechanism of the anticancer action of AAs mainly involves target pathways, including PI3K/AKT, Mitogen-activated protein kinases (MAPKs), Wnt/ $\beta$ -catenin, and nuclear factor  $\kappa$ B (NF- $\kappa$ B) and they induce cell autophagy, apoptosis, and cell cycle arrest (Fig. 4).

##### PI3K-AKT signaling pathway

The activation of the PI3K-AKT signaling pathway is considered as a key factor for cell survival, growth, and resistance to chemotherapy, resulting in cancer development. Particularly, the activated PI3K catalyzes the conversion of PIP2 to PIP3, which results in the activation of AKT by the phosphorylated PIP3, further promoting various biological effects such as cell proliferation and apoptosis by activating downstream effector molecules.

Nuciferine inhibited the metastasis and migration of lung cancer cells by targeting sex determining region Y (SRY)-box 2 (SOX2), a transcription factor that positively associated with the drug-resistant property. Subsequently, nuciferine inactivated the AKT and STAT3 pathway, inhibited EMT while promoted mesenchymal-to-epithelial transition (MET) through down-regulating the expression of Slug and up-regulating the expression of N-cadherin and vimentin [2]. Nuciferine was also found to inhibit angiogenesis through downregulation of the expression of the CD133 (stemness marker), Bcl-2, hypoxia-inducible factor-1 ((HIF1 $\alpha$ ), an angiogenesis marker) and vascular endothelial growth factor A (VEGF-A) [2]. The co-treatment of isocorydine (0.4 mg/kg, IP) and gemcitabine also downregulated the expression of EMT-related transcription factors and STAT3, an upstream mediator of EMT, ultimately inhibiting metastasis, migration, and viability of breast cancer cells [106]. The analysis of the Traditional Chinese Medicine network pharmacology revealed to Qi et al. [96] that nuciferine (9.5 mg/mL, IP) works against human neuroblastoma and mouse colorectal cancer through inactivating of the PI3K-



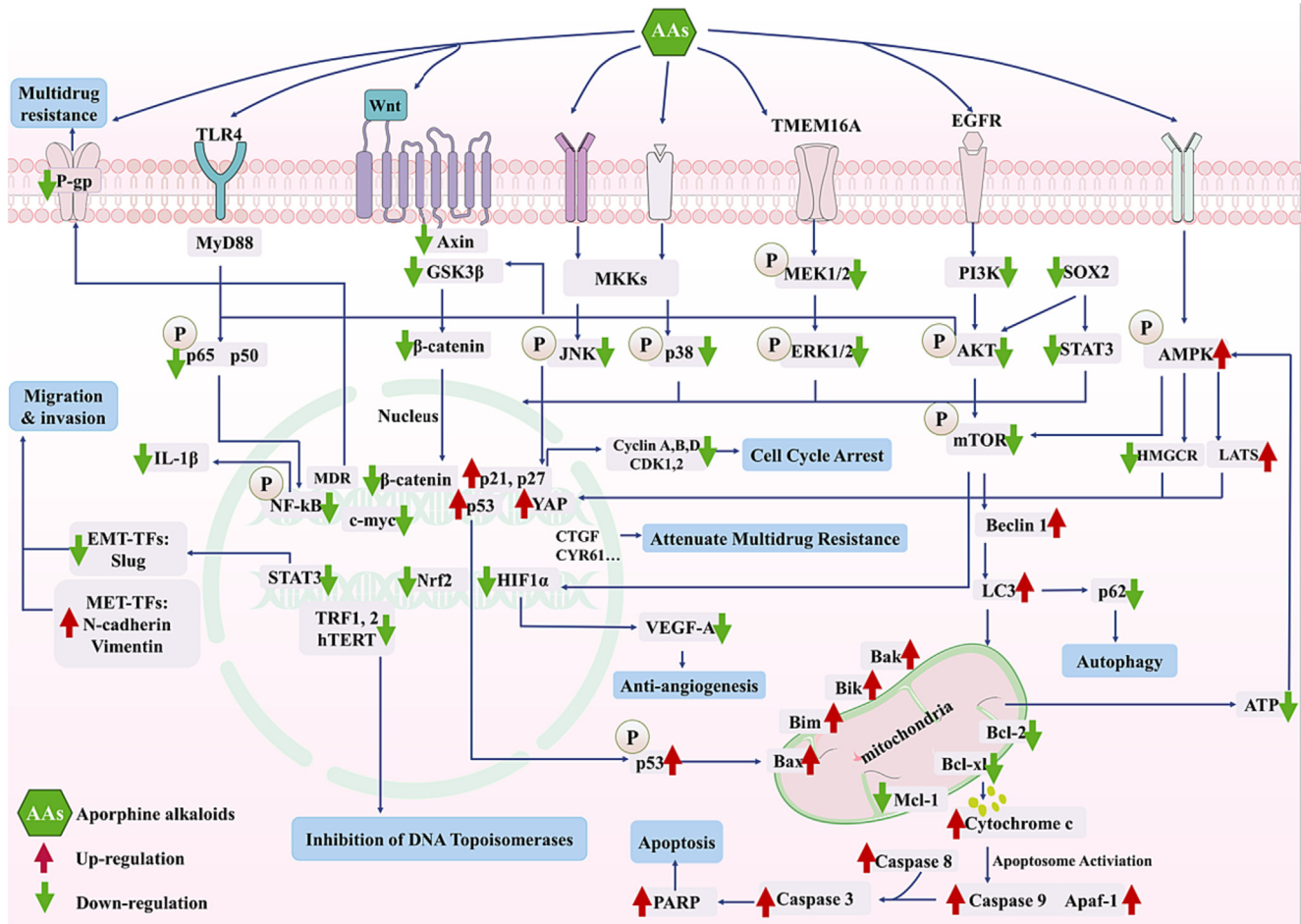


**Fig. 4.** Anticancer mechanisms of AAs. AAs: Aporphine alkaloids; AKT: protein kinase B; AMPK: AMP-activated protein kinase; Apaf-1: the apoptotic protease activating factor-1; CDK1/2: cyclin dependent kinases 1/2; EMT: epithelial-to-mesenchymal transition; ERK: extracellular signal-regulated kinases; EGFR: epidermal growth factor receptor; GSK-3β: glycogen synthase kinase 3β; HMGR: 3-hydroxy-3-methyl-glutaryl-coA reductase; HIF-1α: hypoxia-inducible factor-1 α; hTERT: human telomerase reverse transcriptase; IL: interleukin; JNK: stress-activated protein kinases; mTOR: mechanistic target of rapamycin; MET: mesenchymal-to-epithelial transition; NF-κB: nuclear factor κB; Nrf2: the nuclear factor E2-related factor 2; PI3K: phosphatidylinositol 3-kinase; P-gp: P-glycoprotein; STAT3: activator of transcription 3; SOX2: sex determining region Y (SRY)-box 2; TLR4: Toll-like receptor 4; TMEM16A: the transmembrane protein 16A; VEGF-A: vascular endothelial growth factor A; YAP: YES-associated protein Ser127.

AKT signaling pathway and inhibiting the expression of IL-1β. Nuciferine (7.5 mg/kg, IP) inhibited p-AKT and p-ERK and subsequently down-regulated the downstream targets, including Nrf2, HIF-1α, P-gp, and BCRP, indicating a positive linkage with the multidrug resistance to paclitaxel [108].

Magnoflorine (10 mg/kg, IP) was found to be effectively promoting autophagy of diverse tumor cells through inactivating the PI3K/AKT/mTOR signaling and up-regulating autophagy proteins, including the p62, beclin-1 and LC3-II [110]. Besides, the co-treatment of magnoflorine (3 mg/kg, IP) and doxorubicin has been shown not only to reduce the cardiotoxicity of doxorubicin, but also to promote autophagy in tumor progression [20]. An aristolactam analogue named KO-202125 (0.078–1.95 mg/kg, intragastric administration) inhibited the activity of epidermal growth factor receptor (EGFR), a marker of poor prognosis in many types of cancer, and downregulation of the PI3K/AKT pathway as well as its downstream signals in breast cancer cells, such as glycogen synthase kinase 3β (GSK-3β) and p27 [111].

**MAPK signaling pathway**

MAPKs signaling pathway is one of the most important cellular mechanisms responsible for cell proliferation and mainly includes three subfamilies: ERK1/2, p38, and stress-activated protein

kinases (JNK). As an ion channel protein overexpressed in various cancers, the R515, L522, and E624 amino acid residues of the transmembrane protein 16A (TMEM16A) proposed by molecular docking experiments was inhibited by nuciferine (30 μM, oral). And the phosphorylation of MEK1/2 and ERK1/2 (MAPK signaling) was also inhibited by nuciferine in LA795 Cells [2]. Additionally, the expression of p38 MAPK was markedly activated by the treatment of nuciferine, which induced cell cycle arrest (decreased cyclin dependent kinases 1/2 (CDK1/2) and cyclin B1, increased p53 and p21 expression), apoptosis (decreased Bcl-2 and increased cleaved caspase-9 and 3) and autophagy (increased beclin-1 and LC3) [20,112].

In the gastric cancer mice model, magnoflorine (10 mg/kg, IP) remarkably activated JNK phosphorylation through the regulation of reactive oxygen species (ROS), while had no influence on p38 and ERK1/2, and further induced cell cycle arrest (increased p21 and p27, and decreased cyclin-A and cyclin-B1) and apoptosis (increased cleaved caspase-3 and cleaved poly-ADP-ribose polymerases), inhibiting human gastric cancer progression [110]. However, magnoflorine inhibited lipopolysaccharide-induced macrophages inflammatory responses via blocking the MAPK signaling pathways (attenuated the phosphorylation of p65, ERK, JNK, and p38). At present, the interaction between magnoflorine, macrophage and immune response is still not clear, whereas

lipopolysaccharide-induced inflammation was indeed inhibited by the inactivation of the MAPK signaling pathways [113]. Furthermore, numerous studies demonstrated a crosstalk between various pathways, for example, both the phosphorylations of JNK and p38 were activated by boldine (90 mg/kg, oral) in a dose-dependent manner and maintain a dynamic balance. The inhibition of mouse mammary carcinoma by boldine was associated with the proapoptotic effect of JNK and p38 kinases and antiapoptotic action of ERK1/2 [114].

#### Wnt/ $\beta$ -catenin signaling

The abnormal regulation of the transcription factor  $\beta$ -catenin in the canonical Wnt signaling pathway induces diverse physiological processes such as cellular proliferation and differentiation.  $\beta$ -catenin regulates apoptotic proteins such as Bcl-2 and/or Bax and  $\beta$ -catenin is also regulated by a multiprotein complex, including Axin, adenomatous polyposis coli, and GSK-3 $\beta$ . Of note, several AAs perform their therapeutic effect by targeting the Wnt/ $\beta$ -catenin signaling in cancer. A previous work showed that nuciferine (50 mg/kg, IP) degraded  $\beta$ -catenin through Axin (a vital scaffold protein) accumulation and stabilization, and further suppresses Wnt/ $\beta$ -catenin signaling pathway through the downregulation of the targeted factors including c-myc, cyclin D and VEGF-A. In addition, it exerted pro-apoptosis effects through downregulating Bcl-2 and upregulating Bax, consequently resulting in the suppression of proliferation, metastasis, and growth of non-small cell lung cancer cells [97].

#### NF- $\kappa$ B signaling pathway

The NF- $\kappa$ B plays a well-known role in controlling inflammation, immunity, proliferation, and cell death, and growing evidence supports that NF- $\kappa$ B signaling pathway is activated in many cancers. The regulation of NF- $\kappa$ B signaling pathway is generally accomplished by the key protein p65, and TLR4, a member of the toll-like receptor family, assisting in the initiation of the innate immune response [115,116]. As a hopeful natural product used for dietary adjuvant therapy, nuciferine (50 mg/kg, oral) inhibited melanoma cell growth by reducing p65 phosphorylation and downregulating TLR4 expression in a dose-dependent manner, ultimately inhibiting the NF- $\kappa$ B signaling pathway [117]. Meanwhile, good binding ability of magnoflorine with inflammation cytokines, like TNF- $\alpha$ , IL-6, IL-1 $\beta$ , and MCP-1, was identified by molecular docking analysis. The inactivation of NF- $\kappa$ B signaling induced by magnoflorine was also identified in recent study [113].

#### Cell autophagy, apoptosis, and cycle arrest

Autophagy eliminates cytotoxic materials to exert cytoprotection through the lysosomal degradation pathway and plays an important role in limiting cancer initiation. Apoptosis is generally triggered by the intrinsic (mitochondrial) or the extrinsic (death receptor) pathway to induce cell death and guarantee normal cell turnover. The induction of cell cycle arrest is a valuable strategy in tumor inhibition, which can be regulated by CDKs and cyclins.

The cotreatment with magnoflorine and doxorubicin induced breast cell death *in vivo* by upregulating Beclin-1 and LC3-II and downregulating p62, ultimately leading to autophagosome formation. Additionally, this cotreatment inhibited cell proliferation by upregulating the expression of p53 and p21, resulting in the decreased expression of CDK1, CDK2, and cyclin B, ultimately activating the mitochondrial apoptosis pathway [20,118]. Isocorydine (20 mg/kg, SC or 0.4 mg/kg, IP) inhibited hepatocellular carcinoma cell growth by upregulating the programmed cell death 4 (PDCD4,

a tumor suppressor protein). Besides, isocorydine induced cell cycle arrest and intrinsic apoptosis through downregulating CDKs and antiapoptotic proteins, such as Bcl-2, Bcl-xL, and Mcl-1, and upregulating proapoptotic protein expression, such as Bax, Bim, Bik, and Bak [99,119]. Indeed, the excellent anticancer activity of d-isocorydine (100–250 mg/kg, IP), highlights the significance of the C8 position on the basic skeleton of simple aporphines as a key modifying site, such as amino, carbonyl, and acetyl amino group, described in the section 5.2 [35,100]. It suggests that further exploration and modification of this particular position may lead to the development of even more potent anticancer agents within the AA class.

The anti-cancer mechanism of action for many AAs involves upregulating the apoptotic protease activating factor-1 (Apaf-1), caspase 9 and 3, as well as the poly ADP ribose polymerase (PARP, an apoptotic protein), all of which play significant roles in apoptosis and programmed tumor cell death. Many AAs exerted anticancer activities by regulating these factors, including boldine (50–100 mg/kg, IP or 90 mg/kg, intragastric administration) [94,120], 7-Hydroxydehydronuciferine (20 mg/kg, IP) [121], apomorphine (50  $\mu$ M) [19], and d-isocorydine (100–250 mg/kg, IP), as well as oxoisoaporphine complexes [104,105]. Metal-alkaloid complexes, such as yttrium (III) and dysprosium (III) oxoglucine, have been shown to inhibit the malignant proliferation of HepG2 cells through the degradation of Cdc25A and subsequent inactivation of CDK2 [95].

Additionally, the development of topoisomerase inhibitors represents a hopeful approach to targeting DNA therapy. A chiral platinum complex derivative of oxoaporphine successfully inhibited the growth of HepG2 cells by interacting with p53 binding protein 1 (53BP1), TRF1, c-myc, TRF2 and human telomerase reverse transcriptase (hTERT), targeting DNA and suppressing topoisomerase I activity, leading to S-phase arrest and apoptosis via the mitochondrion-mediated pathway [105]. In addition, the simple aporphines, such as isocorydine [99], magnoflorine [118], xylopin [122], dicentrine [123], boldine and its derivatives [124,125], and an oxoAA liriodenine, [25] inhibited DNA topoisomerases, and induced cell cycle arrest and apoptosis through modulating hTERT, p53, Bax, Bcl-2 and caspase 3, 9, 8 with intrinsic and extrinsic pathways to limit tumor progression. Oxocrebaine, a simple aporphine isolated from *Stephania hainanensis*, was a novel dual topoisomerase inhibitor of Topo I and II $\alpha$ . Oxocrebaine also induced autophagy by increasing the LC3-II/I ratio, Beclin-1 expression and autophagosome formation. It is a dual topoisomerase inhibitor with potential therapeutic applications [126]. Besides, oxostephanine played dual roles in inhibiting aurora kinase activity and angiogenesis [127]. Both docking and molecular dynamics simulations indicated that boldine and the derivative (N-benzylsecoboldine hydrochloride) [124], 4,5-dehydro-9-methoxy guatterfriesine [128], guadiscine and guadiscidine [129] inhibited telomerase activity by regulating the transcription of the catalytic subunit, telomerase reverse transcriptase.

Notably, the inhibition ability of topoisomerases is tightly associated with the planar conformations of compounds. Qing et al. [23] proposed that the conjugation and planar conformation of simple aporphine ring system should be extended by dihydroxy- and oxo- groups, enabling dihydroxyaporphine and oxoAAs to easily intercalate into DNA and inhibiting topoisomerases. Besides, certain substitution groups, namely 1,2-methylenedioxy, N-methyl, and N-2-hydroxypropyl groups, were found to be the crucial factor in enhancing the anticancer activity of AAs. Conversely, the compounds with a ruptured C-ring and a lengthy N-chain, or those substituted with hydroxyl or methyl group at the C7 position, and methyl or acetyl group at nitrogen, as well as quaternary nitrogen on their skeletons, had an adverse effect [23].

## Regulation of gut microbiota

Preclinical and clinical evidence suggests that gut microbiota is an important regulator of cancer development, progression, metastasis and treatment response [130]. Accordingly, the microbiota is gaining increasing attention in cancer diagnosis and treatment. Oral treatment of berberine improved brain dopa/dopamine levels through interactions with the gut microbiota, leading to the amelioration of Parkinson's disease symptoms in patients with hyperlipidemia. The fecal transplantation studies in Parkinson's disease mice have also revealed that berberine improved the disease by activating the gut-brain axis [131]. At the genus level, nuciferine improved colitis by reducing the abundance of *Bilophila* and *Halomonas* *in vivo*, which were regarded as harmful gut microbes, indicating that nuciferine exerted anti-inflammatory activity through regulating the gut microbiota [21]. At present, lack of literature investigating the specific role of gut microbiota in relation to the anti-cancer activities of AAs. There are tremendous opportunities to elucidate the causal and molecular interactions between gut microbiota and AAs in the context of cancer.

## Other signaling pathways

AMPK is considered as the regulator of metabolism, modulating ATP synthesis and consumption to balance body energy level. Nuciferine shows promise as an adjunctive drug to gemcitabine for treating pancreatic cancer by activating AMPK, which subsequently down-regulates HMGCR and YAP. The latter is a major regulator of the mevalonate pathway and an overexpressed protein that contributes to pancreatic cancer progression. Nuciferine (30 mg/kg, IP) showed promise as an adjuvant drug to gemcitabine for treating pancreatic cancer treatment by activating AMPK, which subsequently down-regulated HMGCR and YAP, a major regulator of the mevalonate pathway and an overexpressed protein in pancreatic cancer progression, respectively [107].

Besides, apomorphine was used as a pre-metastatic drug to treat primary tumors before they spread to the brain because of its ability to inhibit tumor cell migration. [102]. The results showed that brain metastasis initiating cells (BMICs) possessed a distinct genetic profile, and apomorphine's ability to cross the BBB has demonstrated its efficacy in targeting BMICs, with the potential to target neural development systems or related disorders at low IC<sub>50</sub>. Besides, apomorphine (5 mg/kg, SC) greatly attenuated brain metastasis development in apomorphine-treated brains both *in silico* and *in vivo* through the downregulation of 3 genes, *KIF16B*, *SEPWI*, and *TESK2* [102]. Protein-protein interactions were identified as novel therapeutic targets. A simple aporphine dicentrine emerged as the be most effective docked alkaloid against breast cancer by regulating tumor suppressor protein p53 and breast cancer associated protein [132].

Approximately 50 AAs exerted anticancer effects in different cancer types. Among them, isocorydine, nuciferine, boldine, magnoflorine, and their derivatives exhibit pharmacological activities in several cancers, providing a theoretical basis for further in-depth experiment and clinical trials. These AAs mainly inhibited cell proliferation and migration, and induce apoptosis through the PI3K-AKT, MAPK, Wnt/ $\beta$ -catenin, NF- $\kappa$ B pathways to induce cell autophagy, apoptosis, and cell cycle arrest. However, mechanisms involving the AA treatment with microbial are still largely unknown. According to the structure-activity relationship, the strong activity of oxoaporphines, dehydroaporphines and other AAs are attributed to their stable conjugation and planar conformation and special substitution groups (1,2-methylenedioxy, N-methyl and N-2-hydroxypropyl group), which allow their easy intercalation into DNA and inhibit topoisomerases. However, lack

of supporting data from *in vivo* models and clinical trials confirmed the antitumor activity and its mechanisms.

## Conclusion

There is an increased interest in the development of AA drugs targeting various diseases especially cancers. The studies of administration of the AAs *in vivo* show their characteristics, such as fast absorption, poor bioavailability as well as wide tissue distribution, which can be attributed to their small molecular weight, nonpolar hydrocarbon backbones and hydrophobic functional groups like aromatic rings. However, poor oral bioavailability is a major obstacle for the development of AAs. The toxicities of AAs are tightly linked with the dosage and administration ways. Side effects, such as subcutaneous nodules, nausea, and somnolence, are reported by apomorphine treatment with 2–6 mg/kg subcutaneous infusion administration in Parkinson's disease patients, whereas most AAs shows no toxicity with specific models. Strategies on bioavailability and systemic toxicity improvement have been reported, such as changing the ways of administration, developing delivery systems (nanoparticles, liposomes), and co-administration with absorption enhancers [133]. Recently, the effects of metabolic enzymes and gut microbiota on AA metabolism have been identified, therefore, the improvement of AA absorption, especially their metabolism in intestine, would be an important direction to be explored.

Undoubtedly, AAs will continue to attract the attention of scientists due to their potential anticancer activity and demand of alternative chemotherapeutic drugs. Different AAs showed anticancer activities in specific tumor models. Thus, it is essential to fully evaluate the safety, pharmacokinetics, and molecular mechanisms of these AAs. Novel chemical structures and the structure-activity relationship based on the high structural diversity of AAs need to be more explored as well. In particular, new strategies should be established to improve AA bioavailability, ultimately enhancing their therapeutic benefits. Altogether, AAs remain a promising pool for the discovery of various bioactivities that could be effectively further developed in cancer therapy based on clinical studies.

## CRediT authorship contribution statement

**Jing Sun:** Investigation, Writing – original draft. **Xingtian Zhan:** Writing – review & editing, Supervision. **Weimin Wang:** Supervision, Writing – review & editing. **Xiaojie Yang:** Investigation, Writing – review & editing. **Yichen Liu:** Writing – original draft. **Huanzhi Yang:** Investigation, Resources. **Jianjun Deng:** Conceptualization, Supervision. **Haixia Yang:** Supervision, Funding acquisition.

## Declaration of Competing Interest

The authors declare that they have no known competing financial interests or personal relationships that could have appeared to influence the work reported in this paper.

## Acknowledgement

This research is supported by National Key Research and Development Program (2022YFF1100205), the National Natural Science Foundation of China (21978229 and 21676212) and Chinese Universities Scientific Fund (15053342).

## References

- [1] Xia C, Dong X, Li H, Cao M, Sun D, He S, et al. Cancer statistics in China and United States, 2022: profiles, trends, and determinants. *Chin Med J (Engl)* 2022;135(5). doi: <https://doi.org/10.1097/CM9.0000000000002108>.

- [2] Bai X, Liu XY, Li ST, An HL, Kang XJ, Guo S. Nuciferine inhibits TMEM16A in dietary adjuvant therapy for lung cancer. *J Agric Food Chem* 2022;70(12):3687–96. doi: <https://doi.org/10.1021/acs.jafc.1c08375>.
- [3] Byrne S, Boyle T, Ahmed M, Lee SH, Benyamin B, Hyppönen E. Lifestyle, genetic risk and incidence of cancer: a prospective cohort study of 13 cancer types. *Int J Epidemiol* 2023;52(3):817–26. doi: <https://doi.org/10.1093/ije/dyac238>.
- [4] Ren Z, Yang H, Zhu C, Fan D, Deng J. Dietary phytochemicals: As a potential natural source for treatment of Alzheimer's Disease. *Food Innovation and Advances* 2023;2(1):36–43. doi: <https://doi.org/10.48130/FIA-2023-0007>.
- [5] Yang H, Xiao L, Yuan Y, Luo X, Jiang M, Ni J, et al. Procyanidin B2 inhibits NLRP3 inflammasome activation in human vascular endothelial cells. *Biochem Pharmacol* 2014;92(4):599–606. doi: <https://doi.org/10.1016/j.bcp.2014.10.001>.
- [6] Fan W, Zong H, Zhao T, Deng J, Yang H. Bioactivities and mechanisms of dietary proanthocyanidins on blood pressure lowering: A critical review of *in vivo* and clinical studies. *Crit Rev Food Sci Nutr* 2022;1549–7852.
- [7] Atanasov AG, Zotchev SB, Dirsch VM, Orhan IE, Banach M, Röllinger JM, et al. Natural products in drug discovery: advances and opportunities. *Nat Rev Drug Discov* 2021;20(3):200–16. doi: <https://doi.org/10.1038/s41573-020-00114-z>.
- [8] Zhang J, Li D, Tian Q, Ding Y, Jiang H, Xin G, et al. The effect of kiwi berry (*Actinidia arguta*) on preventing and alleviating loperamide-induced constipation. *Food Innovation and Advances* 2023;2(1):1–8. doi: <https://doi.org/10.48130/FIA-2023-0001>.
- [9] Yang H, Rothenberger E, Zhao T, Fan W, Kelly A, Attaya A, et al. Regulation of inflammation in cancer by dietary eicosanoids. *Pharmacol Ther* 2023;248: doi: <https://doi.org/10.1016/j.pharmthera.2023.108455>.
- [10] Newman DJ, Cragg GM. Natural Products as Sources of New Drugs over the Nearly Four Decades from 01/1981 to 09/2019. *J Nat Prod* 2020;83(3):770–803. doi: <https://doi.org/10.1021/acs.jnatprod.9b01285>.
- [11] Sharifi-Rad JA-O, Quspice C, Patra JK, Singh YD, Panda MK, Das G, et al. Paclitaxel: Application in Modern Oncology and Nanomedicine-Based Cancer Therapy. *Oxid Med Cell Longev*. 2021(1942-0994 (Electronic)). doi: <https://doi.org/10.1155/2021/3687700>.
- [12] Smith ER, Wang J, Yang D, Xu X. Paclitaxel resistance related to nuclear envelope structural sturdiness. *Drug Resist Updat* 2022;65: doi: <https://doi.org/10.1016/j.drup.2022.100881>.
- [13] Dhyani P, Quspice C, Sharma E, Bahukhandi A, Sati P, Attri DC, et al. Anticancer potential of alkaloids: a key emphasis to colchicine, vinblastine, vincristine, vindesine, vinorelbine and vincamine. *Cancer Cell Int* 2022;22(1):206. doi: <https://doi.org/10.1186/s12935-022-02624-9>.
- [14] Yx W. Alkaloids: A Handbook of Practical Natural Products. Alkaloids. Beijing: Chemical Industry Press Co., Ltd.; 2005.
- [15] Silva TRC, Rita BH, Raminelli C. Advances Towards the Synthesis of Aporphine Alkaloids: C-Ring Formation via Approaches Based on One- and Two-Bond Disconnections. *Chem Rec* 2022;22(2):e202100246.
- [16] Shang XF, Yang CJ, MorrisNatschke SL, Li JC, Yin XD, Liu YQ, et al. Biologically active isoquinoline alkaloids covering 2014–2018. *Med Res Rev* 2020;40(6):2212–89. doi: <https://doi.org/10.1002/med.21703>.
- [17] Wang F, Zhu N, Zhou F, Lin D. Natural aporphine alkaloids with potential to impact metabolic syndrome. *Molecules* 2021;26(20): doi: <https://doi.org/10.3390/molecules26206117>.
- [18] Zheng H, Han L, Shi W, Fang X, Hong Y, Cao Y. Research Advances in Lotus Leaf as Chinese Dietary Herbal Medicine. *Am J Chin Med* 2022;50(06):1423–45. doi: <https://doi.org/10.1142/S0192415X22500616>.
- [19] Lee J, Ham J, Lim W, Song G. Apomorphine facilitates loss of respiratory chain activity in human epithelial ovarian cancer and inhibits angiogenesis *in vivo*. *Free Radic Biol Med* 2020;154:95–104. doi: <https://doi.org/10.1016/j.freeradbiomed.2020.05.001>.
- [20] Tian W, Xie X, Cao P. Magnoflorine improves sensitivity to doxorubicin (DOX) of breast cancer cells via inducing apoptosis and autophagy through AKT/mTOR and p38 signaling pathways. *Biomed Pharmacother* 2020;121: doi: <https://doi.org/10.1016/j.biopha.2019.109139>.
- [21] Zhu Y, Zhao Q, Huang Q, Li Y, Yu J, Zhang R, et al. Nuciferine Regulates Immune Function and Gut Microbiota in DSS-Induced Ulcerative Colitis. *Front Vet Sci* 2022;9.
- [22] Yq Qu, Qy Z, Xy T, Zheng Gh, Zp Q, Xx T. Effect of nuciferine against the proliferation of cholangiocarcinoma cells through Akt/mTOR/4EBP1-glycolytic pathway. *Nat Prod Res Dev* 2023;35(8):1297–304.
- [23] Qing ZX, Huang JL, Yang XY, Liu JH, Cao HL, Xiang F, et al. Anticancer and reversing multidrug resistance activities of natural isoquinoline alkaloids and their structure-activity relationship. *Curr Med Chem* 2018;25(38):5088–114. doi: <https://doi.org/10.2174/0929867234666170920125135>.
- [24] Karki A, Namballa HK, Alberts I, Harding WW. Structural manipulation of aporphines via C10 nitrogenation leads to the identification of new 5-HT7AR ligands. *Bioorg Med Chem* 2020;28(15): doi: <https://doi.org/10.1016/j.bmc.2020.115578>.
- [25] Nordin N, Majid NA, Hashim NM, Rahman MA, Hassan Z, Ali HM. Liriodenine, an aporphine alkaloid from *Encicanthellum pulchrum*, inhibits proliferation of human ovarian cancer cells through induction of apoptosis via the mitochondrial signaling pathway and blocking cell cycle progression. *Drug Des Devel Ther* 2015;9:1437–48. doi: <https://doi.org/10.2147/DDDT.S77727>.
- [26] Wei YB, Li YX, Song H, Feng XJ. Design, synthesis and anticancer activity of oxoaporphine alkaloid derivatives. *J Enzyme Inhib Med Chem* 2014;29(5):722–7. doi: <https://doi.org/10.3109/14756366.2013.845818>.
- [27] Honda T, Shigehisa H. Novel and efficient synthetic path to proaporphine alkaloids: Total synthesis of (+/-)-stepharine and (+/-)-pronuciferine. *Org Lett* 2006;8(4):657–9. doi: <https://doi.org/10.1021/ol052841m>.
- [28] Latolla N, Hlangothi B. Three new proaporphine alkaloids from *Cissampelos capensis* L.f. and their cytotoxic evaluation. *Nat Prod Res* 2022. doi: <https://doi.org/10.1080/14786419.2022.2146687>.
- [29] Kumar V, Poonam PAK, Parmar VS. Naturally occurring aristolactams, aristolochic acids and dioxoaporphines and their biological activities. *Nat Prod Rep* 2003;20(6):565–83. doi: <https://doi.org/10.1039/b303648k>.
- [30] Lin CH, Ko FN, Wu YC, Lu ST, Teng CM. The relaxant actions on guinea-pig trachealis of atherosperminine isolated from *fissistigma-glaucescens*. *Eur J Pharmacol* 1993;237(1):109–16. doi: [https://doi.org/10.1016/0014-2999\(93\)90099-4](https://doi.org/10.1016/0014-2999(93)90099-4).
- [31] Nasrullah AA, Zahari A, Mohamad J, Awang K. Antiplasmodial alkaloids from the bark of *cryptocarya nigra* (lauraceae). *Molecules* 2013;18(7):8009–17. doi: <https://doi.org/10.3390/molecules18078009>.
- [32] Bin Nadzirin I, Fortuny-Gomez A, Ngum N, Richards D, Ali S, Searcey M, et al. Taspine is a natural product that suppresses P2X4 receptor activity via phosphoinositide 3-kinase inhibition. *Br J Pharmacol* 2021;178(24):4859–72. doi: <https://doi.org/10.1111/bph.15663>.
- [33] Ali G, Cuny GD. 8-, 9-, and 11-aryloxy dimeric aporphines and their pharmacological activities. *Molecules* 2021;26(15): doi: <https://doi.org/10.3390/molecules26154521>.
- [34] Morikawa T, Kitagawa N, Tanabe G, Ninomiya K, Okugawa S, Motai C, et al. Quantitative determination of alkaloids in lotus flower (flower buds of *Nelumbo nucifera*) and their melanogenesis inhibitory activity. *Molecules* 2016;21(7): doi: <https://doi.org/10.3390/molecules21070930>.
- [35] Zhong M, Liu YJ, Liu JX, Di DL, Xu MR, Yang YY, et al. Isostrydine derivatives and their anticancer activities. *Molecules* 2014;19(8):12099–115. doi: <https://doi.org/10.3390/molecules190812099>.
- [36] Li DH, Li JY, Xue CM, Han T, Sai CM, Wang KB, et al. Antiproliferative dimeric aporphinoid alkaloids from the roots of *thalictrum cultratum*. *J Nat Prod* 2017;80(11):2893–904. doi: <https://doi.org/10.1021/acs.jnatprod.7b00387>.
- [37] Singh H, Singh D, Lekhak MM. Ethnobotany, botany, phytochemistry and ethnopharmacology of the genus *Thalictrum* L. (Ranunculaceae): A review. *J Ethnopharmacol* 2023;305: doi: <https://doi.org/10.1016/j.jep.2022.115950>.
- [38] Liu C, Kao C, Wu H, Li W, Huang C, Li H, et al. Antioxidant and anticancer aporphine alkaloids from the leaves of *Nelumbo nucifera* Gaertn. *Cv Rosaplenta Molecules* 2014;19(11):17829–38. doi: <https://doi.org/10.3390/molecules191117829>.
- [39] Mohamed SM, Hassan EM, Ibrahim NA. Cytotoxic and antiviral activities of aporphine alkaloids of *Magnolia grandiflora* L. *Nat Prod Res* 2010;24(15):1395–402. doi: <https://doi.org/10.1080/14786410902906959>.
- [40] Min YD, Choi SU, Lee KR. Aporphine alkaloids and their reversal activity of multidrug resistance (MDR) from the stems and rhizomes of *Sinomenium acutum*. *Arch Pharm Res* 2006;29(8):627–32. doi: <https://doi.org/10.1007/BF02968246>.
- [41] Liu Y, He G, Li H, He J, Feng E, Bai L, et al. Plasma pharmacokinetics and tissue distribution study of roemerine in rats by liquid chromatography with tandem mass spectrometry (LC-MS/MS). *J Chromatogr B Analyt Technol Biomed Life Sci* 2014;969:249–55. doi: <https://doi.org/10.1016/j.jchromb.2014.08.031>.
- [42] Nakamura S, Nakashima S, Tanabe G, Oda Y, Yokota N, Fujimoto K, et al. Alkaloid constituents from flower buds and leaves of sacred lotus (*Nelumbo nucifera*, Nymphaeaceae) with melanogenesis inhibitory activity in B16 melanoma cells. *Bioorg Med Chem* 2013;21(3):779–87. doi: <https://doi.org/10.1016/j.bmc.2012.11.038>.
- [43] Fu L, Dai DC, Yang R, Chen GY, Zheng CJ, Song XM, et al. Two novel aporphine-derived alkaloids from the stems of *Fissistigma glaucescens*. *Fitoterapia* 2021;155: doi: <https://doi.org/10.1016/j.fitote.2021.105036>.
- [44] Li D. Natural deep eutectic solvents in phytonutrient extraction and other applications. *Front. Plant Sci* 2022;13: doi: <https://doi.org/10.3389/fpls.2022.1004332>.
- [45] Strzemiński M, Dresler S, Podkościelna B, Skic K, Sowa I, Załuski D, et al. Effectiveness of Volatile Natural Deep Eutectic Solvents (VNADESs) for the Green Extraction of Chelidonium majus Isoquinoline Alkaloids. *Molecules* 2022. doi: <https://doi.org/10.3390/molecules27092815>.
- [46] Torres-Vega J, Gomez-Alonso S, Perez-Navarro J, Pastene-Navarrete E. Green extraction of alkaloids and polyphenols from *peumus boldus* leaves with natural deep eutectic solvents and profiling by HPLC-PDA-IT-MS/MS and HPLC-QTOF-MS/MS. *Plants (Basel)* 2020;9(2): doi: <https://doi.org/10.3390/plants9020242>.
- [47] Takla SS, Shawky E, Hammada HM, Darwish FA. Green techniques in comparison to conventional ones in the extraction of Amaryllidaceae alkaloids: Best solvents selection and parameters optimization. *J Chromatogr A* 2018;1567:99–110. doi: <https://doi.org/10.1016/j.chroma.2018.07.009>.
- [48] Uwineza PA, Waśkiewicz A. Recent Advances in Supercritical Fluid Extraction of Natural Bioactive Compounds from Natural Plant Materials. *Molecules* 2020. doi: <https://doi.org/10.3390/molecules25173847>.
- [49] Arumugham T, K R, Hasan SW, Show PL, Rinklebe J, Banat F. Supercritical carbon dioxide extraction of plant phytochemicals for biological and environmental applications – A review. *Chemosphere*. 2021;271:129525. doi: <https://doi.org/10.1016/j.chemosphere.2020.129525>.
- [50] Hu C, Gan X, Jia Q, Gao P, Du T, Zhang F. Optimization of supercritical-CO2 extraction and pharmacokinetics in SD rats of alkaloids from *Sophora*

- moorcroftiana seed. *Sci Rep* 2022;12(1):3301. doi: <https://doi.org/10.1038/s41598-022-07278-1>.
- [51] Djapic N. Supercritical Carbon Dioxide Extraction of *Nicotiana tabacum* Leaves: Optimization of Extraction Yield and Nicotine Content. *Molecules* 2022. doi: <https://doi.org/10.3390/molecules27238328>.
- [52] Atwi-Ghaddar S, Zerwette L, Destandau E, Lesellier E. Supercritical Fluid Extraction (SFE) of Polar Compounds from *Camellia sinensis* Leaves: Use of Ethanol/Water as a Green Polarity Modifier. *Molecules* 2023. doi: <https://doi.org/10.3390/molecules28145485>.
- [53] Gan R, Liu Y, Li H, Xia Y, Guo H, Geng F, et al. Natural sources, refined extraction, biosynthesis, metabolism, and bioactivities of dietary polymethoxyflavones (PMFs). *Food Sci Hum Wellness* 2024;13(1):27–49. doi: <https://doi.org/10.26599/FSHW.2022.9250003>.
- [54] Liu Y, Liu H-Y, Li S-H, Ma W, Wu D-T, Li H-B, et al. Cannabis sativa bioactive compounds and their extraction, separation, purification, and identification technologies: An updated review. *TRAC Trends Anal Chem* 2022;149:. doi: <https://doi.org/10.1016/j.trac.2022.116554>116554.
- [55] He Q, Lei Q, Huang S, Zhou Y, Liu Y, Zhou S, et al. Effective extraction of bioactive alkaloids from the roots of *Stephania tetrandra* by deep eutectic solvents-based ultrasound-assisted extraction. *J Chromatogr A* 2023;1689:. doi: <https://doi.org/10.1016/j.chroma.2022.463746>463746.
- [56] Ma W, Lu Y, Hu R, Chen J, Zhang Z, Pan Y. Application of ionic liquids based microwave-assisted extraction of three alkaloids N-nornuciferine, O-nornuciferine, and nuciferine from lotus leaf. *Talanta* 2010;80(3):1292–7. doi: <https://doi.org/10.1016/j.talanta.2009.09.027>.
- [57] Ruan YQ, Xu JH, Chu JB, Shi J, Shi QY. Processing tactics for low-cost production of pure nuciferine from lotus leaf. *Ultrason Sonochem* 2022;86. doi: <https://doi.org/10.1016/j.ultrsonch.2022.106026>.
- [58] Mustafa A, Turner C. Pressurized liquid extraction as a green approach in food and herbal plants extraction: A review. *Anal Chim Acta* 2011;703(1):8–18. doi: <https://doi.org/10.1016/j.aca.2011.07.018>.
- [59] Okiyama DCG, Soares ID, Cuevas MS, Crevelin EJ, Moraes LAB, Melo MP, et al. Pressurized liquid extraction of flavanols and alkaloids from cocoa bean shell using ethanol as solvent. *Food Res Int* 2018;114:20–9. doi: <https://doi.org/10.1016/j.foodres.2018.07.055>.
- [60] Agbo F, Isaacson SH, Gil R, Chiu YY, Brantley SJ, Bhargava P, et al. Pharmacokinetics and comparative bioavailability of apomorphine sublingual film and subcutaneous apomorphine formulations in patients with parkinson's disease and "off" episodes: Results of a randomized, three-way crossover, open-label study. *Neurol Ther* 2021;10(2):693–709. doi: <https://doi.org/10.1007/s40120-021-00251-6>.
- [61] Li Z, Liu J, Li Y, Du X, Li Y, Wang R, et al. Identify super quality markers from prototype-based pharmacokinetic markers of Tangzhiqing tablet (TZQ) based on in vitro dissolution/permeation and in vivo absorption correlations. *Phytomedicine* 2018;45:59–67. doi: <https://doi.org/10.1016/j.phymed.2018.04.001>.
- [62] Gu SY, Zhu GH, Wang YZ, Li Q, Wu X, Zhang JG, et al. A sensitive liquid chromatography-tandem mass spectrometry method for pharmacokinetics and tissue distribution of nuciferine in rats. *J Chromatogr B Analyt Technol Biomed Life Sci* 2014;961:20–8. doi: <https://doi.org/10.1016/j.jchromb.2014.04.038>.
- [63] Wang FG, Cao J, Hou XQ, Li ZY, Qu XL. Pharmacokinetics, tissue distribution, bioavailability, and excretion of nuciferine, an alkaloid from lotus, in rats by LC/MS/MS. *Drug Dev Ind Pharm* 2018;44(9):1557–62. doi: <https://doi.org/10.1080/03639045.2018.1483399>.
- [64] Zou S, Ge Y, Chen X, Li J, Yang X, Wang H, et al. Simultaneous determination of five alkaloids by HPLC-MS/MS combined with micro-SPE in rat plasma and its application to pharmacokinetics after oral administration of lotus leaf extract. *Front Pharmacol* 2019;10. doi: <https://doi.org/10.3389/fphar.2019.01252>.
- [65] Huang X, Hao N, Chen G, Liu S, Che Z. Chemistry and biology of nuciferine. *Ind Crops Prod* 2022;179:. doi: <https://doi.org/10.1016/j.indcrop.2022.114694>114694.
- [66] Ye LH, He XX, You C, Tao X, Wang LS, Zhang MD, et al. Pharmacokinetics of nuciferine and n-nornuciferine, two major alkaloids from *Nelumbo nucifera* leaves, in rat plasma and the brain. *Front Pharmacol* 2018;9. doi: <https://doi.org/10.3389/fphar.2018.00902>.
- [67] Liu Y, Wu X, Mi Y, Zhang B, Gu S, Liu G, et al. PLGA nanoparticles for the oral delivery of nuciferine: preparation, physicochemical characterization and in vitro/in vivo studies. *Drug Deliv* 2017;24(1):443–51. doi: <https://doi.org/10.1080/10717544.2016.1261381>.
- [68] Xue BJ, Zhao YY, Miao Q, Miao PP, Yang XY, Sun GX, et al. In vitro and in vivo identification of metabolites of magnoflorine by LC LTQ-Orbitrap MS and its potential pharmacokinetic interaction in *Coptidis Rhizoma* decoction in rat. *Biomed Chromatogr* 2015;29(8):1235–48. doi: <https://doi.org/10.1002/bmc.3413>.
- [69] Tian X, Li Z, Lin Y, Chen M, Pan G, Huang C. Study on the PK profiles of magnoflorine and its potential interaction in Cortex phellodendri decoction by LC-MS/MS. *Anal Bioanal Chem* 2014;406(3):841–9. doi: <https://doi.org/10.1007/s00216-013-7530-9>.
- [70] Guo CC, Yu CH, Li L, Wang YQ, Wang SJ, Wang WH, et al. Rapid determination of isocorydine in rat plasma and tissues using liquid chromatography-tandem mass spectrometry and its applications to pharmacokinetics and tissue distribution. *Xenobiotica* 2012;42(5):466–76. doi: <https://doi.org/10.3109/00498254.2011.640965>.
- [71] Wei JX, Yu YY, Li YN, Shao J, Li JY, Li LZ, et al. Pharmacokinetics, tissue distribution and excretion of 6-O-demethylmenisporphine, a bioactive oxoisoporphine alkaloid from *Menispermis Rhizoma*, as determined by a HPLC-MS/MS method. *J Chromatogr B Analyt Technol Biomed Life Sci* 2020;1156. doi: <https://doi.org/10.1016/j.jchromb.2020.122297>.
- [72] Bao SH, Geng PW, Wang SH, Zhou YF, Hu LF, Yang XZ. Pharmacokinetics in rats and tissue distribution in mouse of magnoflorine by ultra performance liquid chromatography-tandem mass spectrometry. *Int J Clin Exp Med* 2015;8(11):20168–77.
- [73] Lu W, He LC, Zeng XM. HPLC method for the pharmacokinetics and tissue distribution of taspine solution and taspine liposome after intravenous administrations to mice. *J Pharm Biomed Anal* 2008;46(1):170–6. doi: <https://doi.org/10.1016/j.jpba.2007.08.009>.
- [74] Tan JPK, Voo ZX, Lim S, Venkataraman S, Ng KM, Gao S, et al. Effective encapsulation of apomorphine into biodegradable polymeric nanoparticles through a reversible chemical bond for delivery across the blood-brain barrier. *Nanomedicine* 2019;17:236–45. doi: <https://doi.org/10.1016/j.nano.2019.01.014>.
- [75] Li BJ, Han LM, Cao BY, Yang XY, Zhu XH, Yang B, et al. Use of magnoflorine-phospholipid complex to permeate blood-brain barrier and treat depression in the CUMS animal model. *Drug Deliv* 2019;26(1):566–74. doi: <https://doi.org/10.1080/10717544.2019.1616236>.
- [76] Neef C, van Laar T. Pharmacokinetic-pharmacodynamic relationships of apomorphine in patients with Parkinson's disease. *Clin Pharmacokinet* 1999;37(3):257–71. doi: <https://doi.org/10.2165/00003088-199937030-00004>.
- [77] Aloga RN, Fan Y, Zhang G, Li J, Zhao YJ, Kakila JL, et al. Pharmacokinetics of a multicomponent herbal preparation in healthy Chinese and African volunteers. *Sci Rep* 2015;5. doi: <https://doi.org/10.1038/srep12961>.
- [78] Gao H, Zhang L, Zhu A, Liu XY, Wang TX, Wan MQ, et al. Metabolic profiling of nuciferine in vivo and in vitro. *J Agric Food Chem* 2020;68(48):14135–47. doi: <https://doi.org/10.1021/acs.jafc.0c04668>.
- [79] Wu X-L, Wu M-J, Chen X-Z, Ma H-L, Ding L-Q, Qiu F, et al. Metabolic profiling of nuciferine in rat urine, plasma, bile and feces after oral administration using ultra-high performance liquid chromatography-diode array detection-quadrupole time-of-flight mass spectrometry. *J Pharm Biomed Anal* 2017;140:71–80. doi: <https://doi.org/10.1016/j.jpba.2017.03.022>.
- [80] Ye LH, He XX, Kong LT, Liao YH, Pan RL, Xiao BX, et al. Identification and characterization of potent CYP2D6 inhibitors in lotus leaves. *J Ethnopharmacol* 2014;153(1):190–6. doi: <https://doi.org/10.1016/j.jep.2014.02.014>.
- [81] Tang Z, Luo T, Huang P, Luo M, Zhu J, Wang X, et al. Nuciferine administration in C57BL/6J mice with gestational diabetes mellitus induced by a high-fat diet: the improvement of glycolipid disorders and intestinal dysbacteriosis. *Food Funct* 2021;12(22):11174–89. doi: <https://doi.org/10.1039/D1FO02714I>.
- [82] Lai Y, Kuo T, Chen C, Tsai H, Lee S. Metabolism of dicentrine: Identification of the phase I and phase II metabolites in miniature pig urine. *Drug Metab Dispos* 2010;38(10):1714–22. doi: <https://doi.org/10.1124/dmd.110.033795>.
- [83] Hroch M, Micuda S, Cermanova J, Chladek J, Tomsik P. Development of an HPLC fluorescence method for determination of boldine in plasma, bile and urine of rats and identification of its major metabolites by LC-MS/MS. *J Chromatogr B Analyt Technol Biomed Life Sci* 2013;936:48–56. doi: <https://doi.org/10.1016/j.jchromb.2013.07.009>.
- [84] Chen JZ, Chou GX, Wang CH, Yang L, Bligh SWA, Wang ZT. Characterization of new metabolites from in vivo biotransformation of norisoboldine by liquid chromatography/mass spectrometry and NMR spectroscopy. *J Pharm Biomed Anal* 2010;52(5):687–93. doi: <https://doi.org/10.1016/j.jpba.2010.02.008>.
- [85] Li Y, Zeng RJ, Chen JZ, Wu YB, Chou GX, Gao Y, et al. Pharmacokinetics and metabolism study of isoboldine, a major bioactive component from *Radix Linderae* in male rats by UPLC-MS/MS. *J Ethnopharmacol* 2015;171:154–60. doi: <https://doi.org/10.1016/j.jep.2015.05.042>.
- [86] Tan YF, Wang RQ, Wang WT, Wu Y, Ma N, Lu WY, et al. Study on the pharmacokinetics, tissue distribution and excretion of lauroilsine from *Litsea glutinosa* in Sprague-Dawley rats. *Pharm Biol* 2021;59(1):884–92. doi: <https://doi.org/10.1080/13880209.2021.1944221>.
- [87] Wu WN, McKown LA. The in vitro metabolism of thalicarpine, an aporphine-benzyltetrahydroisoquinoline alkaloid, in the rat API-MS/MS identification of thalicarpine and metabolites. *J Pharm Biomed Anal* 2002;30(1):141–50. doi: [https://doi.org/10.1016/S0731-7085\(02\)00202-9](https://doi.org/10.1016/S0731-7085(02)00202-9).
- [88] Liu LY, Zhou L, Liu XZ, Zou DJ. Effect of hedan tablets on body weight and insulin resistance in patients with metabolic syndrome. *Obes Facts* 2022;15(2):180–5. doi: <https://doi.org/10.1159/000520711>.
- [89] Chaudhuri KR, Leta V. Apomorphine infusion for improving sleep in Parkinson's disease. *Lancet Neurol* 2022;21(5):395–8. doi: [https://doi.org/10.1016/S1474-4422\(22\)00128-4](https://doi.org/10.1016/S1474-4422(22)00128-4).
- [90] Dewey RB, Hutton JT, LeWitt PA, Factor SA. A randomized, double-blind, placebo-controlled trial of subcutaneously injected apomorphine for Parkinsonian off-state events. *Arch Neurol* 2001;58(9):1385–92. doi: <https://doi.org/10.1001/archneur.58.9.1385>.
- [91] Esmaili S, Shahidi G, Hajiakhondi F. Apomorphine induced immune hemolytic anemia. *J Neurol Sci* 2019;405. doi: <https://doi.org/10.1016/j.jns.2019.10.1274>.
- [92] Szalak R, Matysek M, Koval M, Dziedzic M, Kowalczyk-Vasilev E, Kruk-Slomka M, et al. Magnoflorine from *Berberis vulgaris* roots-impact on hippocampal neurons in mice after short-term exposure. *Int J Mol Sci* 2023;24(8). doi: <https://doi.org/10.3390/ijms24087166>.

- [93] Ding C, Dai Z, Yu H, Zhao X, Luo X. New aporphine alkaloids with selective cytotoxicity against glioma stem cells from *Thalictrum foetidum*. *Chin J Nat Med* 2019;17(9):698–706. doi: [https://doi.org/10.1016/S1875-5364\(19\)30084-6](https://doi.org/10.1016/S1875-5364(19)30084-6).
- [94] Subramaniam N, Kannan P, Ashokkumar K, Thiruvengadam D. Hepatoprotective effect of boldine against diethylnitrosamine-induced hepatocarcinogenesis in wistar rats. *J Biochem Mol Toxicol* 2019;33(12). doi: <https://doi.org/10.1002/jbt.22404>.
- [95] Wei JH, Chen ZF, Qin JL, Liu YC, Li ZQ, Khan TM, et al. Water-soluble oxoglauanine-Y(III), Dy(III) complexes: in vitro and in vivo anticancer activities by triggering DNA damage, leading to S phase arrest and apoptosis. *Dalton Trans* 2015;44(25):11408–19. doi: <https://doi.org/10.1039/c5dt00926j>.
- [96] Qi Q, Li R, Li HY, Cao YB, Bai M, Fan XJ, et al. Identification of the anti-tumor activity and mechanisms of nuciferine through a network pharmacology approach. *Acta Pharmacol Sin* 2016;37(7):963–72. doi: <https://doi.org/10.1038/aps.2016.53>.
- [97] Liu W, Yi DD, Guo JL, Xiang ZX, Deng LF, He L. Nuciferine, extracted from *Nelumbo nucifera* Gaertn, inhibits tumor-promoting effect of nicotine involving Wnt/beta-catenin signaling in non-small cell lung cancer. *J Ethnopharmacol* 2015;165:83–93. doi: <https://doi.org/10.1016/j.jep.2015.02.015>.
- [98] Li QH, Sui LP, Zhao YH, Chen BG, Li J, Ma ZH, et al. Tripartite motif-containing 44 is involved in the tumorigenesis of laryngeal squamous cell carcinoma, and its expression is downregulated by nuciferine. *Tohoku J Exp Med* 2021;254(1):17–23. doi: <https://doi.org/10.1620/tjem.254.17>.
- [99] Lu P, Sun HF, Zhang LX, Hou HL, Zhang L, Zhao FY, et al. Carcinomascorydine targets the drug-resistant cellular side population through PDCD4-related apoptosis in hepatocellular carcinoma. *Mol Med* 2012;18(7):1136–46. doi: <https://doi.org/10.2119/molmed.2012.00055>.
- [100] Chen LJ, Tian H, Li M, Ge C, Zhao FY, Zhang LX, et al. Derivate isocorydine inhibits cell proliferation in hepatocellular carcinoma cell lines by inducing G2/M cell cycle arrest and apoptosis. *Tumour Biol* 2016;37(5):5951–61. doi: <https://doi.org/10.1007/s13277-015-4362-6>.
- [101] Menezes LRA, Costa COD, Rodrigues A, Sinto FRD, Nepel A, Dutra LM, et al. Cytotoxic alkaloids from the stem of *Xylopija laevigata*. *Molecules* 2016;21(7). doi: <https://doi.org/10.3390/molecules21070890>.
- [102] Singh M, Venugopal C, Tokar T, McFarlane N, Subapanditha MK, Qazi M, et al. Therapeutic Targeting of the Premetastatic Stage in Human Lung-to-Brain Metastasis. *Cancer Res* 2018;78(17):5124–34. doi: <https://doi.org/10.1158/0008-5472.CCR-18-1022>.
- [103] Qin Q, Qin J, Chen M, Li Y, Meng T, Zhou J, et al. Chiral platinum (II)-4-(2,3-dihydroxypropyl)-formamide oxoaporphine (FOA) complexes promote tumor cells apoptosis by directly targeting G-quadruplex DNA in vitro and in vivo. *Oncotarget* 2017;8(37):61982–97. doi: <https://doi.org/10.18632/oncotarget.18778>.
- [104] Chen ZF, Qin QP, Qin JL, Liu YC, Huang KB, Li YL, et al. Stabilization of G-quadruplex DNA, inhibition of telomerase activity, and tumor cell apoptosis by organoplatinum(II) complexes with oxisoaporphine. *J Med Chem* 2015;58(5):2159–79. doi: <https://doi.org/10.1021/jm5012484>.
- [105] Qin J, Shen W, Chen Z, Zhao L, Qin Q-P, Yu Y, et al. Oxoaporphine metal complexes (Co-II, Ni-II, Zn-II) with high antitumor activity by inducing mitochondria-mediated apoptosis and S-phase arrest in HepG2. *Sci Rep* 2017;7. doi: <https://doi.org/10.1038/srep46056>.
- [106] Zhang QB, Ye RF, Ye LY, Zhang QY, Dai NG. Isocorydine decrease gemcitabine-resistance by inhibiting epithelial-mesenchymal transition via STAT3 in pancreatic cancer cells. *Am J Transl Res* 2020;12(7):3702–14.
- [107] Zhou L, Wang QY, Zhang H, Li YJ, Xie SY, Xu ML. YAP inhibition by nuciferine via AMPK-mediated downregulation of HMGR sensitizes pancreatic cancer cells to gemcitabine. *Biomolecules* 2019;9(10). doi: <https://doi.org/10.3390/biom9100620>.
- [108] Liu RM, Xu P, Chen Q, Feng SL, Xie Y. A multiple-targets alkaloid nuciferine overcomes paclitaxel-induced drug resistance in vitro and in vivo. *Phytomedicine* 2020;79. doi: <https://doi.org/10.1016/j.phymed.2020.153342>.
- [109] Bashir DJ, Manzoor S, Sarfaraj M, Afzal SM, Bashir M, Nidhi, et al. Magnoflorine-Loaded Chitosan Collagen Nanocapsules Ameliorate Cognitive Deficit in Scopolamine-Induced Alzheimer's Disease-like Conditions in a Rat Model by Downregulating IL-1 $\beta$ , IL-6, TNF- $\alpha$ , and Oxidative Stress and Upregulating Brain-Derived Neurotrophic Factor and DCX Expressions. *ACS Omega*. 2023;8(2):2227–36. doi: 10.1021/acsomega.2c06467.
- [110] Sun X, Zhang X, Zhai H, Zhang D, Ma S. Magnoflorine inhibits human gastric cancer progression by inducing autophagy, apoptosis and cell cycle arrest by JNK activation regulated by ROS. *Biomed Pharmacother* 2020;125. doi: <https://doi.org/10.1016/j.biopha.2019.109118>.
- [111] Oh M, Lee J, Shin D, Park J, Oian T, Kim H, et al. The in vitro and in vivo antitumor effect of KO-202125, a sauristolaetam derivative, as a novel epidermal growth factor receptor inhibitor in human breast cancer. *Cancer Sci* 2011;102(3):597–604. doi: <https://doi.org/10.1111/j.1349-7006.2010.01817.x>.
- [112] Wang X, Cheang WS, Yang H, Xiao L, Lai B, Zhang M, et al. Nuciferine relaxes rat mesenteric arteries through endothelium-dependent and -independent mechanisms. *Br J Pharmacol* 2015;172(23):5609–18. doi: <https://doi.org/10.1111/bjph.13021>.
- [113] Wang L, Li PF, Zhou Y, Gu RJ, Lu G, Zhang CB. Magnoflorine Ameliorates Collagen-Induced Arthritis by Suppressing the Inflammation Response via the NF-kappa B/MAPK Signaling Pathways. *J Inflamm Res* 2023;16:2271–96. doi: <https://doi.org/10.2147/JIR.S406298>.
- [114] Tomsik P, Micuda S, Muthna D, Cermakova E, Havelek R, Rudolf E, et al. Boldine inhibits mouse mammary carcinoma in vivo and human MCF-7 breast cancer cells in vitro. *Planta Med* 2016;82(16):1416–24. doi: <https://doi.org/10.1055/s-0042-113611>.
- [115] Qu L, Liu Q, Zhang Q, Tuo X, Fan D, Deng J, et al. Kiwifruit seed oil prevents obesity by regulating inflammation, thermogenesis, and gut microbiota in high-fat diet-induced obese C57BL/6 mice. *Food Chem Toxicol* 2019;125:85–94. doi: <https://doi.org/10.1016/j.fct.2018.12.046>.
- [116] Zhang X, Zhou Y, Cheong MS, Khan H, Ruan C-C, Fu M, et al. Citri Reticulatae Pericarpium extract and flavonoids reduce inflammation in RAW 264.7 macrophages by inactivation of MAPK and NF- $\kappa$ B pathways. *Food Frontiers* 2022;3(4):785–95. doi: <https://doi.org/10.1002/fft.2.169>.
- [117] Xu J, Ying A, Shi T. Nuciferine inhibits skin cutaneous melanoma cell growth by suppressing TLR4/NF-kappa B signaling. *Anticancer Agents Med Chem* 2020;20(17):2099–105. doi: <https://doi.org/10.2174/187152062066620081114607>.
- [118] Okon E, Kukula-Koch W, Jarzab A, Halasa M, Stepulak A, Wawruszak A. Advances in chemistry and bioactivity of magnoflorine and magnoflorine-containing extracts. *Int J Mol Sci* 2020;21(4). doi: <https://doi.org/10.3390/ijms21041330>.
- [119] Sun H, Hou H, Lu P, Zhang L, Zhao F, Ge C, et al. Isocorydine inhibits cell proliferation in hepatocellular carcinoma cell lines by inducing G2/M cell cycle arrest and apoptosis. *PLoS One* 2012;7(5). doi: <https://doi.org/10.1371/journal.pone.0036808>.
- [120] Paydar M, Kamalidehghan B, Wong YL, Wong WF, Looi CY, Mustafa MR. Evaluation of cytotoxic and chemotherapeutic properties of boldine in breast cancer using in vitro and in vivo models. *Drug Des Devel Ther* 2014;8:719–33. doi: <https://doi.org/10.2147/DDDT.S58178>.
- [121] Wu P, Chiu C, Chen C, Wang HD. 7-Hydroxydehydroneuciferine induces human melanoma death via triggering autophagy and apoptosis. *Exp Dermatol* 2015;24(12):930–5. doi: <https://doi.org/10.1111/exd.12805>.
- [122] Santos LS, Silva VR, Alencar Menezes LR, Pereira Soares MB, Costa EV, Bezerra DP. Xylopine induces oxidative stress and causes G2(M) phase arrest, triggering caspase-mediated apoptosis by p53-independent pathway in HCT116 cells. *Oxid Med Cell Longevity* 2017; 2017.. doi: <https://doi.org/10.1155/2017/7126872>.
- [123] Konkimalla VB, Efferth T. Inhibition of epidermal growth factor receptor over-expressing cancer cells by the aporphine-type isoquinoline alkaloid, dicentrine. *Biochem Pharmacol* 2010;79(8):1092–9. doi: <https://doi.org/10.1016/j.bcp.2009.11.025>.
- [124] Noureini SK, Kheirabadi M, Masoumi F, Khosrogerdi F, Zarei Y, Suarez-Rozas C, et al. Telomerase inhibition by a new synthetic derivative of the aporphine alkaloid boldine. *Int J Mol Sci* 2018;19(4). doi: <https://doi.org/10.3390/ijms19041239>.
- [125] Noureini SK, Tanavar F. Boldine, a natural aporphine alkaloid, inhibits telomerase at non-toxic concentrations. *Chem Biol Interact* 2015;231:27–34. doi: <https://doi.org/10.1016/j.cbi.2015.02.020>.
- [126] Yu L, Han S, Lang L, Song H, Zhang C, Dong L, et al. Oxocrebamine: A novel dual topoisomerase inhibitor, suppressed the proliferation of breast cancer cells MCF-7 by inducing DNA damage and mitotic arrest. *Phytomedicine* 2021;84. doi: <https://doi.org/10.1016/j.phymed.2021.153504>.
- [127] Tran THT, Vu LDB, Nguyen HQ, Pham HB, Do XPT, Than UTT, et al. Dual roles of oxostephanine as an Aurora kinase inhibitor and angiogenesis suppressor. *Int J Mol Med* 2022;50(5). doi: <https://doi.org/10.3892/ijmm.2022.5189>.
- [128] Branches ADS, Costa RA, Junior ESA, Bezerra DP, Soares MBP, Costa EV, et al. Theoretical and experimental study by DFT, molecular docking calculations and cytotoxicity assay of 7,7-dimethylaporphine alkaloids type isolated from *Guatteria friesiana* (Annonaceae). *J Mol Struct* 2019;1177:347–62. doi: <https://doi.org/10.1016/j.molstruc.2018.09.060>.
- [129] Costa RA, Barros GA, da Silva JN, Oliveira KM, Bezerra DP, Soares MBP, et al. Experimental and theoretical study on spectral features, reactivity, solvation, topoisomerase I inhibition and in vitro cytotoxicity in human HepG2 cells of guadiscine and guadiscidine aporphine alkaloids. *J Mol Struct* 2021;1229. doi: <https://doi.org/10.1016/j.molstruc.2020.129844>.
- [130] Matson V, Chervin CS, Gajewski TF. Cancer and the Microbiome—Influence of the Commensal Microbiota on Cancer, Immune Responses, and Immunotherapy. *Gastroenterology* 2021;160(2):600–13. doi: <https://doi.org/10.1053/j.gastro.2020.11.041>.
- [131] Wang Y, Tong Q, Ma S-R, Zhao Z-X, Pan L-B, Cong L, et al. Oral berberine improves brain dopa/dopamine levels to ameliorate Parkinson's disease by regulating gut microbiota. *Signal Transduction Targeted Ther* 2021;6(1):77. doi: <https://doi.org/10.1038/s41392-020-00456-5>.
- [132] Tiwari S, Awasthi M, Singh S, Pandey VP, Dwivedi UN. Modulation of interaction of mutant TP53 and wild type BRCA1 by alkaloids: a computational approach towards targeting protein-protein interaction as a futuristic therapeutic intervention strategy for breast cancer impediment. *J Biomol Struct Dyn* 2018;36(13):3376–87. doi: <https://doi.org/10.1080/07391102.2017.1388286>.
- [133] Mollazadeh S, Mackiewicz M, Yazdimamaghani M. Recent advances in the redox-responsive drug delivery nanoplateforms: A chemical structure and physical property perspective. *Mater Sci Eng C Mater Biol Appl* 2021;118. doi: <https://doi.org/10.1016/j.msec.2020.111536>.
- [134] Jin Q, Yang D, Dai Z, Khan A, Wang B, Wei X, et al. Antitumor aporphine alkaloids from *Thalictrum wangii*. *Fitoterapia* 2018;128:204–12. doi: <https://doi.org/10.1016/j.fitote.2018.05.012>.

- [135] Sesang W, Punyanitya S, Pichuanom S, Udomputtimekakul P, Nuntasen N, Banjerdpongchai R, et al. Cytotoxic aporphine alkaloids from leaves and twigs of *pseuduvaria trimera* (craib). *Molecules* 2014;19(7):8762–72. doi: <https://doi.org/10.3390/molecules19078762>.
- [136] Lekphrom R, Kanokmedhakul S, Kanokmedhakul K. Bioactive styryllactones and alkaloid from flowers of *Goniothalamus laoticus*. *J Ethnopharmacol* 2009;125(1):47–50. doi: <https://doi.org/10.1016/j.jep.2009.06.023>.
- [137] Garcez FR, da Silva AFG, Garcez WS, Linck G, Matos MDC, Santos ECS, et al. Cytotoxic aporphine alkaloids from *ocotea acutifolia*. *Planta Med* 2011;77(4):383–7. doi: <https://doi.org/10.1055/s-0030-1250401>.
- [138] Zahari A, Cheah FK, Mohamad J, Sulaiman SN, Litaudon M, Leong KH, et al. Antiplasmodial and antioxidant isoquinoline alkaloids from *dehaasia longipedicellata*. *Planta Med* 2014;80(7):599–603. doi: <https://doi.org/10.1055/s-0034-1368349>.
- [139] Makarasa A, Sirithana W, Mogkhuntod S, Khunnawutmanotham N, Chimnoi N, Techasakul S. Cytotoxic and antimicrobial activities of aporphine alkaloids isolated from *stephania venosa* (blume) spreng. *Planta Med* 2011;77(13):1519–24. doi: <https://doi.org/10.1055/s-0030-1270743>.
- [140] Le PM, Srivastava V, Nguyen TT, Pradines B, Madamet M, Mosnier J, et al. Stephanine from *stephania venosa* (blume) spreng showed effective antiplasmodial and anticancer activities, the latter by inducing apoptosis through the reverse of mitotic exit. *Phytother Res* 2017;31(9):1357–68. doi: <https://doi.org/10.1002/ptr.5861>.
- [141] Thijssen E, Den Heijer JM, Puijert D, Van Brummelen EMJ, Naranda T, Jan GG. Safety and pharmacokinetics of multiple dosing with inhalable apomorphine (AZ-009), and its efficacy in a randomized crossover study in Parkinson's disease patients. *Parkinsonism Relat Disord* 2022;97:84–90. doi: <https://doi.org/10.1016/j.parkreidis.2022.02.014>.
- [142] Zhou J, Sun JB, Zheng P, Liu J, Cheng ZH, Zeng P, et al. Orthogonal array design for optimization of hollow-fiber-based liquid-phase microextraction combined with high-performance liquid chromatography for study of the pharmacokinetics of magnoflorine in rat plasma. *Anal Bioanal Chem* 2012;403(7):1951–60. doi: <https://doi.org/10.1007/s00216-012-6013-8>.
- [143] Lu JZ, Hong DD, Ye D, Mu S, Shi R, Song Y, et al. Tissue distribution and integrated pharmacokinetic properties of major effective constituents of oral Gegen-Qinlian decoction in mice. *Front Pharmacol* 2022;13. doi: <https://doi.org/10.3389/fphar.2022.996143>.
- [144] Lu YL, He YQ, Wang MA, Zhang L, Yang L, Wang ZT, et al. Characterization of nuciferine metabolism by P450 enzymes and uridine diphosphate glucuronosyltransferases in liver microsomes from humans and animals. *Acta Pharmacol Sin* 2010;31(12):1635–42. doi: <https://doi.org/10.1038/aps.2010.172>.
- [145] Qin Q, Qin J, Meng T, Lin W, Zhang C, Wei Z, et al. High in vivo antitumor activity of cobalt oxoisoaporphine complexes by targeting G-quadruplex DNA, telomerase and disrupting mitochondrial functions. *Eur J Med Chem* 2016;124:380–92. doi: <https://doi.org/10.1016/j.ejmech.2016.08.063>.
- [146] Lin H, Huang H, Liao J, Shen C, Huang R. Dicentrine analogue-induced G2/M arrest and apoptosis through inhibition of topoisomerase II activity in human cancer cells. *Planta Med* 2015;81(10):830–7. doi: <https://doi.org/10.1055/s-0035-1546128>.
- [147] Yodkeeree S, Pompimon W, Limtrakul P. Crebanine, an aporphine alkaloid, sensitizes TNF- $\alpha$ -induced apoptosis and suppressed invasion of human lung adenocarcinoma cells A549 by blocking NF- $\kappa$ B-regulated gene products. *Tumour Biol* 2014;35(9):8615–24. doi: <https://doi.org/10.1007/s13277-014-1998-6>.

Jing SUN received her master degree from Northwest University of Food Science and Technology in 2022. Now she is a doctoral student in China Agricultural University of Food Science and Nutrition Engineering. Currently, her research primarily focuses on the hepatoprotective effects of natural products.

Xingtian Zhan obtained his bachelor degree from Southeast University of biological engineering in 2015, now he is a doctoral student majoring in Social Medicine and Health Management in Renmin University of China. Currently his research primarily focuses on the health economics and health policy.

Weimin WANG obtained his bachelor degree of Food Science and Engineering from Hefei University of Technology in 2022, now he is a master candidate of China Agricultural University. Currently his research primarily focuses on the nutrition and chronic disease prevention.

Xiaojie YANG received her bachelor degree from Jiangnan University of Food Science and Engineering in 2022, now she is a master candidate of China Agricultural University. Currently her research primarily focuses on the nutrition and chronic disease prevention.

Yichen LIU obtained her bachelor degree from South-Central Minzu University of Food Quality and Safety in 2022, now she is a master candidate of China Agricultural University. Her research primarily focuses on the analysis of the nutritional composition of *Lycium barbarum* seeds and the effect of UHP on their polyphenols.

Huanzhi YANG graduated from Hunan Agricultural University in 2018 with a master's degree in bioengineering. In 2019, he studied at the College of Food Science and Nutrition Engineering of China Agricultural University as a doctoral student in Food Science.

Jianjun DENG obtained his PhD in food biotechnology from China Agricultural University in 2010. He completed his post-doctoral training at the University of Hong Kong and Harvard Medical School. He is currently a professor of School of Chemical Engineering in Northwest University. His research interests include natural products and chronic disease prevention and control, food chemistry and nutrition, fatty acid metabolism and cancer. He has published more than 130 academic papers and is currently an associate editor of *eFood* and a guest editor of *Nutrients and Antioxidants*.

Haixia YANG received her PhD in Food Science College from China Agricultural University in 2011. She studied as a postdoc research fellow in University of Massachusetts Amherst and Harvard Medical School. Now she is a professor working at the College of Food Science and Nutritional Engineering from China Agricultural University. She has published more than 100 papers related to the food science, including protein purification and function, phytochemicals and inflammation-associated diseases and cancer. She is currently an editor of *Frontiers in Nutrition, Nutrients, Antioxidants, and Protein & Peptide Letters*.